UNIVERSITÀ DEGLI STUDI DI NAPOLI FEDERICO II

PH.D. THESIS

IN

INFORMATION AND COMMUNICATION TECHNOLOGY FOR HEALTH

MACHINE LEARNING FOR HEALTH

A CASE STUDY IN COLORECTAL SURGERY

ANTONIO SCIUTO

TUTOR: PROF. EGIDIO DE BENEDETTO

COORDINATOR: PROF. DANIELE RICCIO

XXXVI CICLO

SCUOLA POLITECNICA E DELLE SCIENZE DI BASE
DIPARTIMENTO DI INGEGNERIA ELETTRICA E TECNOLOGIE DELL'INFORMAZIONE

"While the development of precision surgery will benefit many patients, it is worth to underscore that in the era of biology-driven decisions and high-tech diagnostic and therapeutic tools, the surgeon must remain a medical doctor providing compassionate care through a clinical approach based on direct personal interaction with patients."

– Ugo Boggi

Abstract

Colorectal diseases including cancer and several benign conditions lead to a significant number of surgical procedures worldwide. Today, these surgeries are commonly performed using a minimally invasive approach, such as laparoscopy or robot-assisted surgery. Reduced blood flow to the remaining healthy bowel is associated with significant postoperative complications, which negatively affect patient outcomes and increase healthcare costs. In recent years, near-infrared imaging using indocyanine green fluorescence has become a promising tool for intraoperative assessment of bowel perfusion. Temporal trend of fluorescence rather than its intensity may better predict the onset of complications. However, one major limitation of this technique is that fluorescence evaluation relies on the surgeon's subjective interpretation. Intraoperative decisions based on indocyanine green fluorescence angiography are influenced by the surgeon's experience and exhibit a considerable interindividual variation. Artificial intelligence is increasingly being explored as a powerful instrument in the surgical field to improve precision and ultimately enhance operative performance and patient outcomes. Due to its subjective nature, fluorescence assessment of bowel perfusion may benefit from the application of machine learning, a subset of artificial intelligence that enables computers to learn from and make predictions or decisions based on data. The objective of this research work is to investigate the feasibility of a machine learning-based decision-support system that can automatically evaluate the quality of perfusion during colorectal surgery. For this purpose, surgical videos were collected and preprocessed to reduce the impact of environmental factors. Randomly chosen regions of interest were tracked in the video frames to extract fluorescence intensity-time curves. Unsupervised machine learning methods including K-means and self-organizing map were developed to obtain curve patterns. This provides a starting point to perform risk labelling on each pattern and feed a neural network that may classify a bowel area as adequately or inadequately perfused. Such a system could facilitate efficient and objective decision-making in the operating room.

Contents

Introduction

Colorectal resection involves surgical removal of all or part of the large bowel to treat some common conditions such as cancer or benign diseases. A minimally invasive approach through laparoscopic or robot-assisted surgery is typically used for colorectal procedures. Following resection, the remaining healthy ends of the bowel are connected together using a suture known as an "anastomosis". Several factors influence the healing of the anastomosis. Failure to heal can result in anastomotic leakage (AL), which leads to the flow of bowel contents into the abdominal cavity. AL is the most feared complication of colorectal surgery since it is associated with significant morbidity, mortality, reduced patient quality of life, shorter survival after cancer surgery, and higher healthcare costs. Blood flow reduction at the anastomotic site is associated with an increased risk of leakage. Therefore, it is crucial to assess bowel perfusion during the surgical procedure in order to reduce the risk of this complication.

In recent years, advanced imaging technologies have emerged as an important tool to guide surgical procedures. In this setting, fluorescence imaging using near-infrared technology and indocyanine green (ICG), a tricarbocyanine iodide dye molecule, has become a promising tool for intraoperative assessment of bowel perfusion. Despite some limitations, current studies suggest that ICG fluorescence angiography (ICG-FA) may reduce the incidence of AL following colorectal surgery. However, one major limitation is that fluorescence evaluation relies on the surgeon's subjective interpretation of the amount, uniformity, and speed at which the green dye diffuses in the bowel wall. Therefore, decisions based on intraoperative ICG-FA are affected by surgeon's experience and exhibit a significant interindividual variation.

The use of digital technology is widespread in the surgical field and artificial intelligence (AI) is an integral part of digital surgery. AI has the potential to revolutionize surgery by using data to improve precision and ultimately enhance patient outcomes, operative performance, and the efficiency of surgeons. Machine learning (ML) is a subset of AI that focuses on automatically learning insights and recognizing patterns from data. Although still in their early stages, especially in the field of colorectal surgery, ML algorithms have been proposed as a potentially valuable tool for intraoperative decision-making and guidance.

Due to its subjective nature, ICG-based assessment of bowel perfusion may benefit from the application of AI. The objective of this research work is to investigate the feasibility of a decision-support system that can automatically evaluate the quality of perfusion. Such a system can inform the surgical strategy to minimize the risk of AL, which negatively impact on patients, surgeon, and healthcare system. For this purpose, surgical videos retrieved during minimally invasive colorectal procedures performed at both a university and a community hospital have been used.

The thesis is structured into four chapters, each addressing a different aspect of the topic. In the first part, the clinical setting for the work and the applications of AI in the surgical field are discussed. In the last two chapters, the proposed algorithm and its results are presented.

Chapter 1

Clinical setting

Surgical resection is usually required for a variety of benign and malignant conditions of the colon and rectum, including diverticulitis, inflammatory bowel diseases, colonic volvulus and ischemia, pelvic floor disorders and constipation, severe infectious colitis, polyps not amenable to endoscopic removal, and, most notably, colorectal cancer. Over the last decades, there has been a growing trend in using minimally invasive techniques for colon and rectal surgeries. These techniques enable procedures to be performed through multiple small incisions, resulting in reduced trauma and faster postoperative recovery compared to traditional open surgery (1).

With the advancement of technology, colorectal surgeons have become interested in using intraoperative fluorescence imaging to guide surgical procedures. Fluorophores allow for the real-time visualization of anatomical structures and provide information that is typically difficult to perceive with the naked eye. ICG was approved for medical use in the late 1950s and is widely employed to assess bowel blood supply during colon and rectal resections (2).

The purpose of this chapter is to explain the clinical background for the thesis work.

1.1 Surgery of the colon and rectum

Colorectal diseases lead to a significant number of surgical procedures in colorectal and general surgery units worldwide. A wide range of operations are performed to treat colorectal conditions that require surgery. In the following sections, the principles of anatomy and surgical technique as well as minimally invasive approaches to colorectal surgery will be discussed.

1.1.1 Surgical anatomy

The large bowel, approximately 150 cm long, is the distal part of the digestive tract. It is responsible for absorbing water and electrolytes, producing and absorbing vitamins, and forming and moving feces for elimination through the anus (3). The large bowel extends from the distal end of the terminal ileum to the anus and includes the cecum, colon proper, rectum, and anal canal. The colon proper can be divided into different segments, namely ascending, transverse, descending, and sigmoid, as shown in Fig. 1.1. The curve between the ascending and transverse colon is called hepatic flexure, while the curve between the transverse and descending colon is called splenic flexure. The cecum,

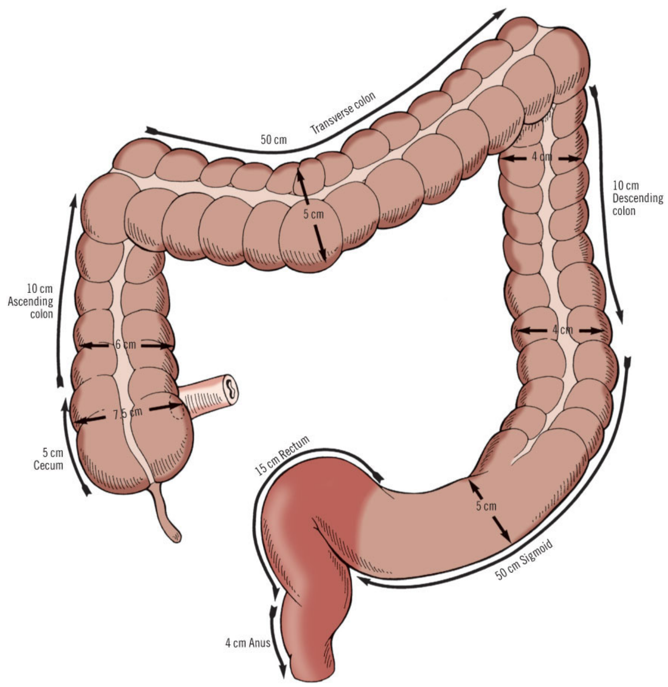

Fig. 1.1 Structure of the large bowel (4)

ascending colon, and the proximal two-thirds of the transverse colon form a surgical unit known as right colon. On the other hand, the distal transverse colon and the descending and sigmoid colons constitute the left colon (4).

The peritoneum is a thin serous membrane that lines the abdominal wall and organs. A peritoneal fold called mesocolon encloses the colon and connects it to the posterior abdominal wall. The mesocolon has a core of loose connective tissue and contains fat, lymph nodes, lymphatic and blood vessels, and nerves that supply the colon. The mesocolon is continuous from the ileocecal junction to the rectosigmoid junction. At this point, it extends into a similar structure that surrounds the rectum, which is referred to as the mesorectum (5).

The colon receives its blood supply from the superior and inferior mesenteric arteries. Branches from the superior mesenteric artery (ileocolic, right colic and middle colic arteries) supply the right colon, while the left colon is supplied by branches from the inferior mesenteric artery (left colic and sigmoid arteries). The boundary between the two arterial supplies is the splenic flexure. Branches from the mesenteric arteries form interconnected arcades that give rise to a single looping vessel known as the marginal artery of Drummond. This lies in the mesocolon and runs roughly parallel to the bowel, about 1 to 8 cm from the intestinal wall (Fig. 1.2). Occasionally, however, the continuity of this artery is disrupted in one or more points. The rectum and anal canal receive blood from various sources. These include the superior rectal artery, which continues from the inferior mesenteric artery, as well as branches of the internal iliac artery (middle and inferior rectal arteries) and aorta (median sacral artery).

The distribution of the veins of the large intestine resembles that of its arteries. Then, the veins from the colon and the superior rectal vein drain into the portal system, whereas the middle and inferior rectal veins along with the median sacral vein drain into the systemic circulation.

The lymph nodes of the large intestine have been divided into four groups: epicolic, under the serosa of the wall of the intestine; paracolic, along the marginal artery; intermediate, along the main arteries; and principal, at the root of the superior and inferior mesenteric arteries. Some of the lymphatic drainage from the lower rectum and anal canal goes to the hypogastric and inguinal nodes (4,6).

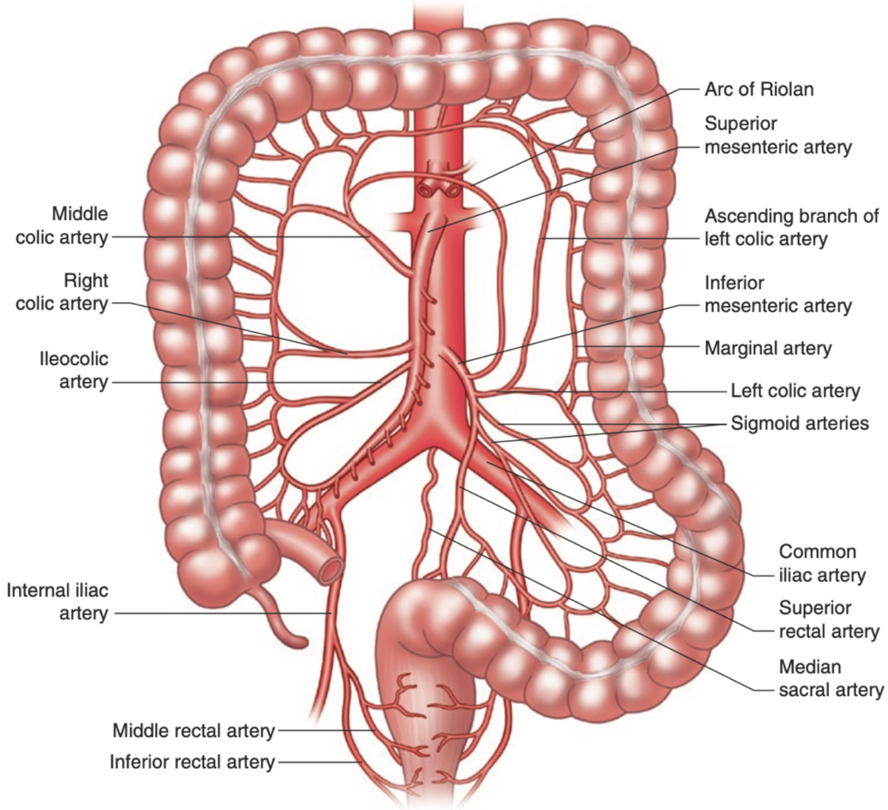

Fig. 1.2 Arterial anatomy of the colon and rectum (6)

1.1.2 Principles of colorectal resections

Colon resection is a surgical procedure in which either a part or the entire colon is removed along with the corresponding mesocolon. The length of the bowel as well as the width of the mesocolon that are removed depend on the condition that requires surgery (7).

Malignancy is the commonest indication for surgical resection of the colon and necessitates a wide resection of the entire tumor-bearing bowel segment supplied by a major artery. The corresponding mesocolon is removed at its root, in order to include almost all the lymphatic drainage of the bowel segment. Thus, the location of the tumor along with the main vascular supply determine the type of colectomy to be performed (6). Tumors located in the right colon should be removed with a right colectomy, which involves resection of a portion of the distal ileum, cecum, ascending colon, and proximal to mid-transverse colon. Extended right hemicolectomy refers to extension of the distal resection margin to include the distal transverse colon up to the splenic flexure. Tumors of the left colon should be removed with a left colectomy, extending from the descending (or distal transverse) colon to the upper rectum (Fig. 1.3). For tumors located at the splenic flexure, a segmental resection extending from the distal transverse to the sigmoid colon can be performed. Less extensive resections of the bowel as well as the mesocolon may be performed for benign conditions such as trauma, diverticular disease, colitis, inflammatory bowel disease. Regardless of the extent of colon removal, the marginal artery of Drummond is interrupted at the same level as

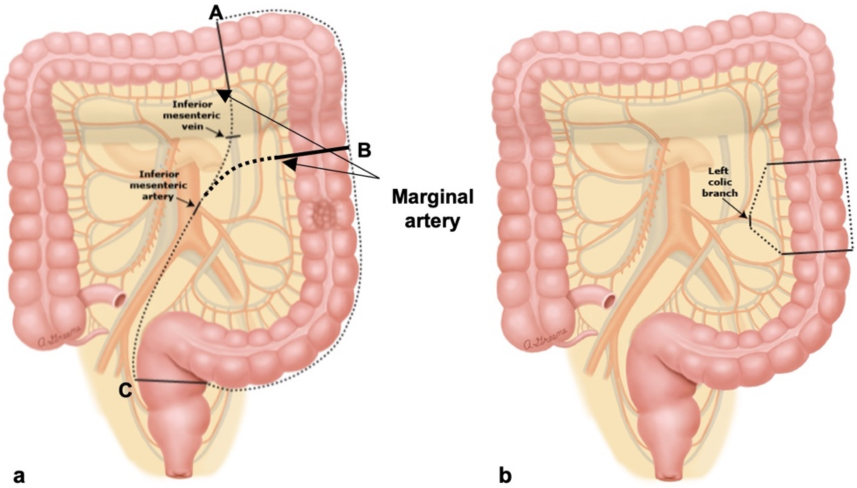

Fig. 1.3 Left colectomy for malignant disease (a). The mesocolon is depicted in yellow. The inferior mesenteric artery is ligated at its origin. The bowel is divided proximally at the descending (B) or less commonly transverse (A) colon and distally at the upper rectum (C). Vascular supply to the colonic stump is provided by the marginal artery, which is divided at the same level of colonic transection. In panel (b), a limited resection for benign disease is shown. Adapted from (8)

where the colon is cut. For certain diseases, a more extensive removal of the colon may be necessary, such as a total or subtotal colectomy (8).

Surgery is the cornerstone of curative therapy for rectal cancer. A local excision may be performed transanally for early tumors. However, most tumors require a radical excision. This is performed transabdominally with either an anterior resection of the rectum or an abdominoperineal resection (Miles' operation). Anterior resection involves removal of the sigmoid colon and either part or the entire rectum dependently on the tumor location. This procedure also entails partial or total removal of the mesorectal envelope, while preserving the anal sphincter complex (9). On the other hand, abdominoperineal resection involves removal of the sigmoid colon, rectum, and anus. Indications include low-lying rectal cancer involving the anal sphincter complex or in patients with fecal incontinence, anal cancer, and inflammatory bowel diseases. Finally, total proctocolectomy refers to surgical removal of the entire colon and rectum (10).

After removing the diseased bowel segment, the proximal and distal ends of the bowel are usually connected through an anastomosis to restore the continuity of the digestive tract. The term "anastomosis" refers to any suture line joining two hollow conduits (11). When intestinal continuity cannot be restored, a stoma is performed. This involves exteriorization of either small bowel (ileostomy) or large bowel (colostomy) through the anterior abdominal wall (12).

After right colectomy, an anastomosis between the terminal ileum and transverse colon (ileo-colic anastomosis) is created. On the other hand, both left colectomy and anterior rectal resection involve fashioning an anastomosis between the descending colon and rectum, named as colorectal anastomosis.

Anastomoses are created using different methods, with the choice of technique typically based on the surgeon's preference. Hand-sewn anastomoses have become less common as the use of intestinal stapling devices has increased. Modern surgical gastrointestinal staplers have evolved from the first 1950s-era Russian prototypes. Linear staplers place two linear triple rows of staggered staples and divide the tissue between the rows. They are used to construct side-to-side anastomoses as well as to cut the bowel and close it on both sides of the section line. Circular staplers are used to construct end-to-end or end-to-side anastomoses. The stapler consists of a tubular body and a removable anvil. To create a colorectal anastomosis, the body of the stapler is inserted through the anus and pushed to the end of the rectal stump, which has been closed with a linear stapler. The anvil is secured within the colon by tying a purse-string suture tightly around the connecting end of the anvil. The spike in the body of the circular stapler is extended under direct vision through the closed end of the rectal stump. The connecting end of the anvil is placed onto the spike, and the stapler is closed and fired, producing a circular anastomosis of two or three concentric rows of staggered staples. The stapler contains a circular knife that removes the excess tissue (13). The process of creating an anastomosis using a circular stapler is shown in Figure 1.4.

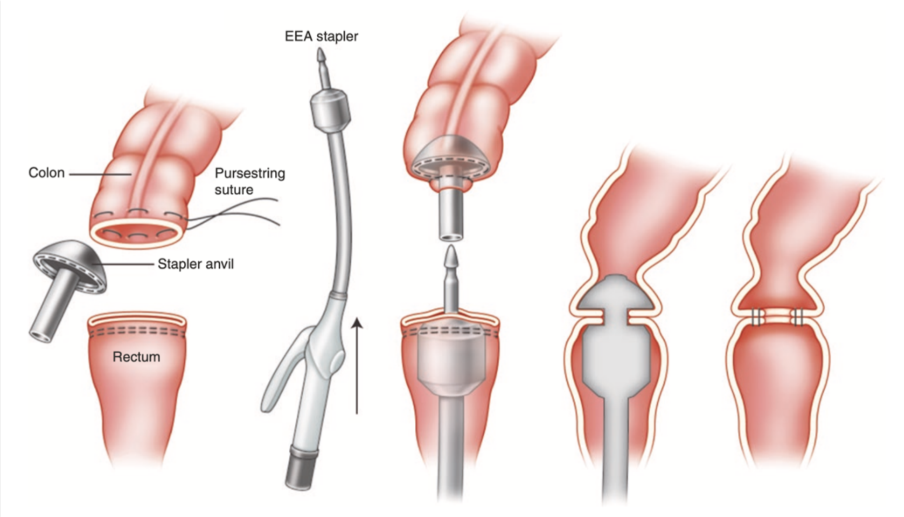

Fig. 1.4 Construction of an end-to-end anastomosis with a circular stapler during left colectomy or anterior rectal resection

1.1.3 Minimally invasive surgery

The collaboration between surgical innovators, biomedical engineers, industry, and the growing patient demand led to the development of what is known as minimally invasive surgery (14). This term is commonly used to describe endoscopic, laparoscopic, and more recently, robotic surgery. The word "laparoscopy" derives from the Greek word *λαπάρα* (lapara) which means "flank" or abdomen and *σκοπέω* (skopeo) meaning "to look at" or examine. Laparoscopy is a surgical approach that involves inserting a visualization device (laparoscope) and surgical instruments through small ports to perform the procedure (15).

The first laparoscopic colectomies were reported by surgeons Jacobs, Verdeja, and Goldstein in 1991(16). Laparoscopy has been a major revolution in colorectal surgery, although it has taken several years to become a popular approach due to the great complexity of laparoscopic colorectal resections (17). However, over a span of more than thirty years, this approach has been proven to enhance short-term postoperative outcomes when compared to open surgery. Laparoscopy is associated with less blood loss, quicker bowel recovery, shorter time to resume oral intake, less analgesic consumption, fewer wound complications, shorter hospital stay, earlier return to regular activity, and better cosmetic results. In addition, long-term evidence of oncologic safety has been demonstrated for the laparoscopic treatment of colorectal cancer (18,19).

In laparoscopy, the abdomen is inflated with carbon dioxide (pneumoperitoneum) to create a working space. Pneumoperitoneum also helps to separate anatomical structures. To prevent the loss of the working space, instruments are inserted through trocars or ports that are placed through small incisions (5 or 12 mm) in the abdominal wall. These ports are equipped with gaskets that create a seal around the instruments. The instrument handles are located outside the patient, while the shafts are long, which reduces tactile feedback. Because laparoscopic instruments are placed through trocars that are fixed in the abdominal wall, this creates a lever or fulcrum effect, which limits the range of motion to six directions (up, down, right, left, clockwise, or counterclockwise rotation). Working with long instruments across a fulcrum can amplify any existing tremor, making it difficult to perform procedures that require fine movements. The laparoscope illuminates the target tissues and provides a magnified, high-definition image to the entire surgical team through an attached or incorporated camera system. Laparoscopes are available with either a straight (0°) or angled (30°) tip. Laparoscopic imaging typically provides a monocular view, as opposed to the binocular view in open surgery, because traditional laparoscopes use a single-lens system. The surgeon obtains a two-dimensional view of the abdominal cavity and its structures displayed on a video monitor. However, three-dimensional and, more recently, ultra-high-definition (4K) technology has been developed to improve the depth perception in laparoscopic surgery (20). Laparoscopes can be used to capture still images or videos for documentation, research, or teaching. These images can be stored either locally on a physical hard drive, desktop viewing station, and onsite picture archiving and communication system (PACS) or using cloud storage solutions. A drawback of laparoscopy is the limited field of view; the laparoscope must be moved to maintain an ideal image. The closer the laparoscope image is to the target, the better the illumination, magnification, and image detail, but the field of view is more limited (21).

After laparoscopy became integrated into surgical practice, the next step in this revolutionary process was the adoption of robot-assisted surgery at the dawn of the new millennium. Colorectal procedures for benign disease (22) as well as for colon cancer (23) were first reported in 2002.

The word "robot" is derived from the Czech noun "robota", which describes forced labor or activity and appeared almost a century ago in the science-fiction play *R.U.R. Rossumovi univerzální roboti* (R.U.R. Rossum's Universal Robots) by the novelist Karel Čapek (24).

Unlike the use of robotics in industry, most surgical applications do not involve autonomous robots. Instead, the robot serves as an interface between the operating surgeon and patient. In this master-slave relationship, the master (surgeon) sits at a console, in an ergonomic and comfortable position, and uses movements of both hands and feet to control movement of the laparoscope and instruments (slave) in the patient. Robot-assisted surgery was designed to overcome most of the technical limitations of conventional laparoscopy, potentially enhancing the capabilities of the surgeon when compared with working freehand (21). Its application to colorectal surgery has shown some operative advantages for surgeons. However, it is often challenging to prove clear advantages for patients. This is partly due to the rapid development of technology, which outpaces the ability of high-quality studies to validate the results (24).

The da Vinci® system is the most widely used multiport robotic platform. However, as technology continues to advance and many patents expire, new robotic platforms are being introduced to the market or awaiting regulatory approval (25).

The da Vinci® system presents three main components: a surgical console, a vision cart, and a patient cart (Fig. 1.5). The surgical console

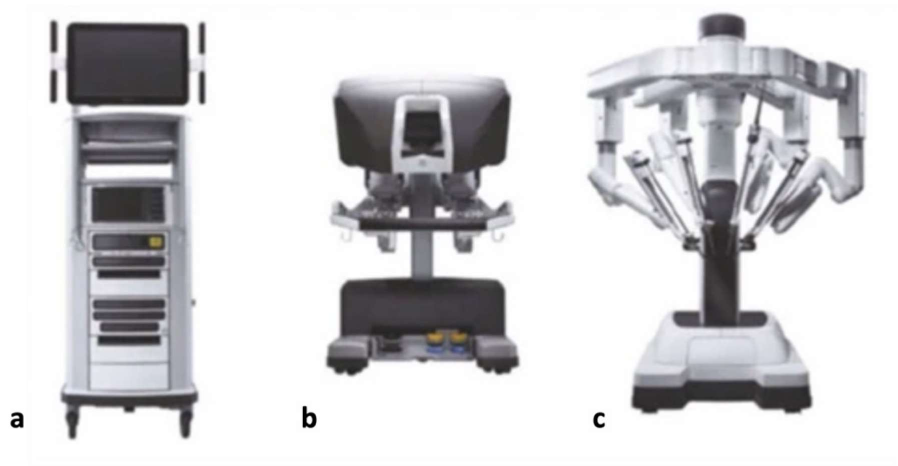

Fig. 1.5 Components of the da Vinci® surgical system: (a) vision cart; (b) console; (c) patient cart (26)

consists of a stereoscopic viewer providing an immersive binocular vision of the operative field; a touchpad for system configuration; master control handles to drive the instrument arms; foot pedals to control electric devices, to switch or release instrument arms, and to move the camera. The patient-side moveable cart supports the robotic arms for instruments and camera, which are inserted in the abdominal wall through 8 or 12-mm cannulas. The robotic arms use remote center technology, where the arms and cannulas move around a fixed point in space, minimizing the force exerted on the patient's abdominal wall. The instruments are wristed near their distal tips and provide seven degrees of freedom (EndoWrist® technology). These are depth adjustment of the instrument tip, side-to-side and up and down rotation of the instrument around the remote center (via the instrument arm), rotation of the instrument shaft around its own central axis, side-to-side and up and down rotation (via the instrument wrist) as well as opening and closing of the instrument jaws. This technology imitates the human wrist and provides surgeon with natural dexterity, eliminating the fulcrum effect that exists in conventional laparoscopy. Aligning the instrument tip with hand movement (intuitive motion) enables the replication of the experience of open surgery, while motion scaling and tremor filtration improve accuracy and precision. One drawback is that the surgeon cannot rely on tactile feedback but must use visual information. The vision cart includes the image processing and vision equipment, a touchscreen for system settings, and adjustable shelves for other surgical devices like insufflators and electrosurgical generators. Available with either a straight (0°) or angled (30°) tip, the da Vinci® endoscope has two separate optical channels and focusing elements. The camera head also includes two separate cameras, providing a magnified, three-dimensional, high-definition image with accurate depth perception.

In 2011, the FireFly® imaging system was developed and integrated into the da Vinci® platform. The system can emit an infrared excitation laser light through the endoscope and detect the infrared signal from fluorescing ICG. Software algorithms colorize the fluorescence signal. Commands at the surgical console enable real-time switching between normal white light and near-infrared (NIR) light modes. This feature enables fluorescence-guided surgery to be performed (26). Similarly, NIR telescopes, and more recently, integrated imaging platforms have been developed for laparoscopic surgery.

1.2 Anastomotic leakage

Every colorectal surgeon during his or her career is faced with anastomotic leakage (AL); the most dreaded complications due to its unpredictability, variable clinical presentation, and significant impact on postoperative outcomes (27,28).

AL is defined as a defect of the intestinal wall at the anastomotic site (including suture and staple lines of neorectal reservoirs) leading to a communication between the intra- and extraluminal compartments (29). Leak occurs when an anastomosis fails to heal, resulting in the flow of bowel contents into the abdominal cavity (Fig. 1.6).

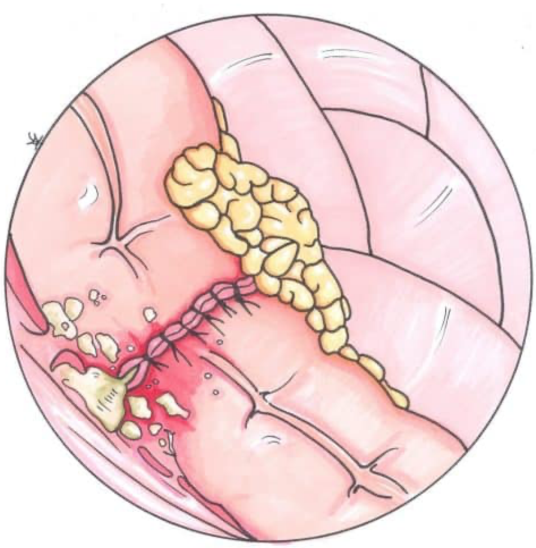

Fig. 1.6 Anastomotic leakage (30)

AL has a wide range of clinical features ranging from a radiological only finding to systemic symptoms (e.g., accelerated heart rate, tachypnea, and oliguria) or even life-threatening conditions such as peritonitis, and sepsis with multiple organ failure. Based on the patient presentation, leaks may not require active intervention or may be managed with either non-operative intervention (e.g., antibiotics, radiologic placement of a pelvic drain) or surgery (31).

In the postoperative period, leakage remains a strong negative determinant of early outcomes. It significantly increases the morbidity, mortality, readmission, and reoperation rates, while significantly prolonging length of hospital stay (32). But leak also impact heavily on late results by causing stricture formation at the anastomotic site, significantly decreasing survival rates after cancer surgery, condemning patients to live with often permanent stomas, and finally by hugely increasing the cost of care (28,33,34).

Leak rates have been found to vary according to the anatomic location of the anastomosis, with distal colorectal, coloanal, and ileoanal anastomoses leaking in up to 20% of cases. The etiology of AL is multifactorial, which makes it challenging to accurately predict the perioperative risk of leakage (35). The integrity of any anastomosis created at any site along the gut depends on four main factors: the patient, the bowel, the surrounding milieu, and the surgeon (Table 1.1).

Patient	**Bowel**	**Milieu**	**Surgeon**
Nutrition (albumin level)	Edema (e.g., after massive fluid resuscitation; decreased venous outflow)	Infection of the space where anastomosis lies (e.g., peritonitis, empyema)	Too much tension on anastomosis (i.e., poor surgical judgement)
Cardiovascular stability (shock)	Inflammation (e.g., inflammatory bowel disease)	Severe inflammation adjacent to the anastomosis (e.g., acute necrotizing pancreatitis)	Anastomosis not watertight/airtight (i.e., faulty technique)
Respiratory status (hypoxiemia)	Poor perfusion (e.g., vasculitis)	No parietal cover leading to exposed anastomosis (loss of abdominal wall, laparostomy)	Stapler disfunction – due to faulty device or improper use
Uremia		Abdominal compartment syndrome (decreased mesenteric perfusion)	
Chronic steroid intake			
Cytotoxic drugs			
Non-steroidal anti-inflammatory drugs (NSAIDs) intake			
Uncontrolled diabetes			
Smoking			

Table 1.1 Common factors influencing anastomotic healing or leaking (36)

Intraoperatively, the following cardinal principles must be obeyed to perform a good anastomosis: the blood supply to the anastomosed bowel must be meticulously preserved; only healthy bowel ends should be joined; before creating the anastomosis, the bowel ends should come together comfortably and without tension; the anastomosis must provide a seal against liquid and gas (36).

Good bowel perfusion is a major contributing factor for the complete healing of the anastomosis. Blood flow reduction at the anastomotic site is associated with an increased risk of anastomotic failure (37). Thereby, evaluation of bowel perfusion at the anastomotic site may have a useful role in reducing the rates of AL. Traditionally perfusion assessment has been performed visually and manually by surgeons. They rely on the color of the tissue, peristalsis, bleeding from the resection line, and palpation of the mesenteric pulse to determine if the visceral perfusion is acceptable. However, these methods are limited when performing minimally invasive surgery. Furthermore, this traditional assessment is susceptible to the clinician's experience and has low accuracy. Over the years, various methods to assess intestinal microcirculation, e.g., X-ray angiography, spectroscopy, doppler ultrasound, and laser Doppler velocimetry, have been suggested but not incorporated into routine practice due to technical complexity, poor reproducibility, and high costs (38). In recent years, NIR fluorescence technology with ICG has emerged as the most promising method that provides a real-time assessment of intestinal perfusion (39).

1.3 Indocyanine green

Indocyanine green (ICG) has been approved by the U.S. Food and Drug Administration (FDA) for clinical and research use in humans since 1956. ICG is a tricarbocyanine iodide dye molecule that is amphiphilic (Fig. 1.7). It can be either used either intravenously or through targeted injections into the tissues. Intravenously injected ICG quickly binds to plasma proteins, such as albumin, globulins, and lipoproteins. As a result, approximately 95% to 98% of ICG remains within the bloodstream. The dye is quickly cleared by the liver with a rate of 18%

to 24% per minute. This leads to a half-life of generally 3 to 4 minutes depending on the vascularization of the organ of interest. ICG is virtually nontoxic, provided the patient does not have an iodide allergy (40).

In the 1970s, it was discovered that protein-bound ICG emits fluorescence peaking at approximately 830 nm when irradiated with NIR light of approximately 750-800 nm wavelength (41). ICG is not selective to specific tissues but can highlight tissues with fluorescence when perfused into the tissues or excreted from the liver or kidney (42).

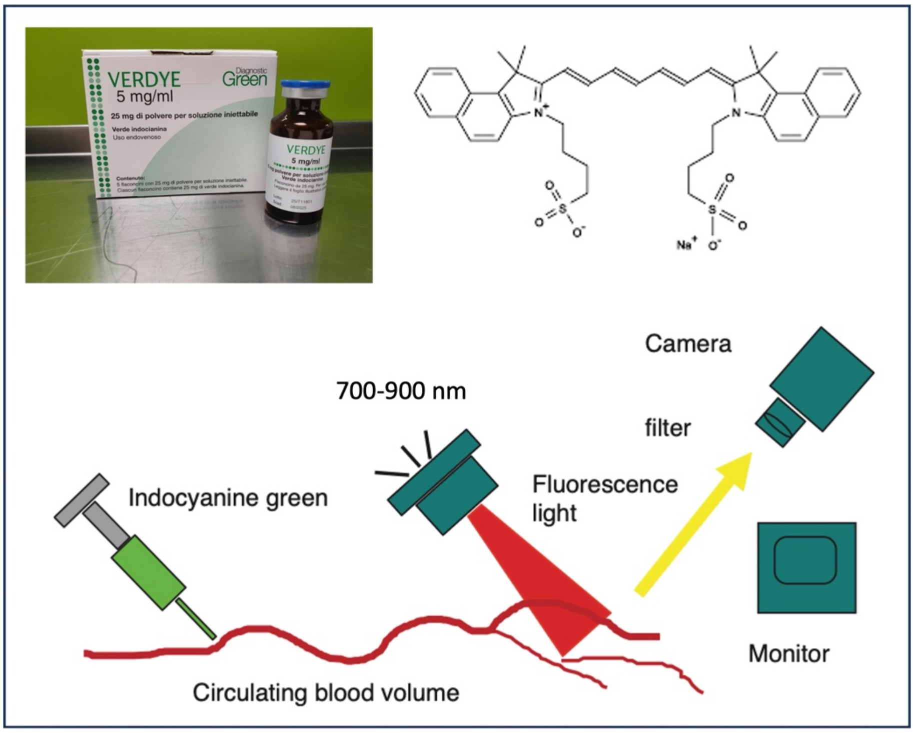

Fig. 1.7 Indocyanine green. After intravenous injection, the region of interest is illuminated with near-infrared light. The fluorescence emission of the excited dye is detected by an infrared-sensitive camera (43)

ICG fluorescence has been widely used for over forty years to examine liver function, microcirculation, and ophthalmic angiography

(43). Since the 2000s, fluorescent capabilities have increasingly been used to provide intraoperative information in various surgical specialties, such as neurosurgery, plastic surgery, gynecology, and general surgery (44). As the human eye cannot detect light at NIR wavelengths, the fluorescent agent does not interfere with the standard surgical field and can be used for intraoperative imaging with a camera system capable of excitation and detection of the fluorescent contrast. In the operating room, a white light camera is used to capture real-world images, while a second NIR camera is used to capture the fluorescence images emitted by the dye. Both cameras can be integrated into a single system (42,44).

In the field of colorectal surgery, ICG can be applied for multiple functions such as tumor localization, lymphatic mapping, intraoperative angiography, as well as detection of peritoneal carcinomatosis and prevention of iatrogenic ureteral injuries (45–47).

ICG-based assessment of bowel perfusion, also known as ICG fluorescence angiography (ICG-FA), is the most used application. During ICG-FA, the well perfused colonic segments appear clearly fluorescent in contrast to the poorly perfused segments that exhibit delayed or no fluorescence. ICG-FA can be performed either inside or outside the abdomen in low-light conditions by turning off the operating room lighting (45). Perfusion can be evaluated before bowel resection to ensure a proper transection line and confirm adequate blood flow to the remaining bowel (Fig. 1.8). Based on the results of fluorescence angiography, surgeons can change the transection line to a more fluorescent and better perfused segment. After completing the anastomosis, another ICG injection can be performed to visualize the integrity and blood flow to the anastomosis (48).

To date, several studies have been conducted to determine if ICG-FA is an effective tool for reducing the occurrence of leakage. However, high-quality evidence has been lacking in terms of reaching definitive conclusions. Although ICG-FA is becoming an extremely widespread technique, it is applied with considerable variability regarding the fluorescence systems that are used, the type or resection requiring assessment, the dose and dilution of ICG, and the timing of injection. These issues hinder the collection of accurate multicentric data, which

Fig. 1.8 ICG fluorescence angiography before bowel transection. (a) Bowel under white light. (b) Fluorescence image. Note the clear distinction between the well-perfused (green) and non-vascularized (grayish) colon.

is necessary for obtaining high-quality evidence on the effectiveness of this technique (49). The largest and most comprehensive review on the role of ICG-FA in colorectal anastomosis assessment included 27 studies entailing more than 8,000 patients. Assessment of colorectal anastomoses with ICG-FA was associated with significantly lower odds of AL (OR 0.452; 95% CI 0.366-0.558) and complications (OR 0.747; 95% CI 0.592-0.943) than inspection under white light. The weighted mean rate of change in surgical plan based on ICG-FA was 9.6% (95% CI 7.3-11.8) and varied from 0.64% to 28.75% across the studies (50). In addition, a meta-analysis of three randomized controlled trials including almost 1,000 patients found that ICG-FA was significantly protective against AL (RR: 0.67, 95% CI 0.46-0.99), although the magnitude of the effect was small (51). From the hospital payer's perspective, a cost analysis demonstrates that based on recent publications of leak rates and cost of colorectal resections, the routine use of ICG-FA for perfusion assessment is a cost-saving measure (52).

The explanation of lower leak rates with the use of ICG-FA is reasonably attributed to the ability of the surgeons to recognize sub-optimally perfused bowel segments, which may otherwise appear healthy under white light (50).

It is noteworthy that despite the benefit of ICG-FA in reducing the rates of colorectal AL, this technique is not entirely objective. The assessment remains at the discretion of the operating surgeon, relying on his/her subjective interpretation of the on-screen images to guide decision-making. Hardy et al. investigated the inter-user variation in the interpretation of NIR imaging among forty surgeons with different levels of experience in ICG-FA. Surgeons were asked to either choose the colonic transection line or judging bowel perfusion based on ICG fluorescence. Regarding colonic transection, overall agreement was higher among expert users than non-experts, while there was no interpretation concordance among any cohort when judging ICG perfusion sufficiency on a yes/no basis. Moreover, most experts felt that more than 50 cases are required for competency in the use of ICG-FA. This study confirms that ICG-FA is prone to variable interpretation. Variability may decline with increasing user experience, although the learning curve is longer than a few initial cases. These findings support the development of methods to provide real-time quantitative decision support. Such systems may shorten the learning curve and increase the yield of fluorescence imaging for users of all experience levels (53).

Chapter 2

Digital surgery

The healthcare industry is currently facing several challenges including increasingly high costs of healthcare services, professionals, and equipment; shortage of skilled professionals in the face of a rising demand for high-quality healthcare services; size and complexity of the healthcare value chain; the need for collaboration among healthcare providers, supporting industries, and organizations; and intense competition among healthcare providers. These challenges are prompting healthcare providers to consider incorporating and using new healthcare models that utilize innovative and advanced information and communication technology. The integration of new information technologies into the healthcare domain resulted in what is known as Health 4.0. This is a newly coined concept that is developed from Industry 4.0, which represents the fourth manufacturing revolution and aims to enhance operations, reduce costs, and improve quality through optimization, industrial automation, and the use of intelligent services (54,55). Health 4.0 is a term used to describe the digital transformation occurring in the sector of health concurrently with Industry 4.0. The aim of Health 4.0 is to offer advanced, valuable, and cost-effective healthcare services to patients while also enhancing the efficiency and productivity of the healthcare industry (56). Health 4.0 focuses on moving healthcare services from being based on "empirical data" to "precision medicine", which involves personalized healthcare services (54). Categories of Health 4.0 are shown in Figure 2.1.

The use of digital technology is widespread in the surgical field. Its uptake is not limited to the operating room alone, but has an increasing role in different domains, such as preoperative planning, surgical risk prediction, and surgical performance assessment. An expert consensus recently defined digital surgery as "the use of technology for the

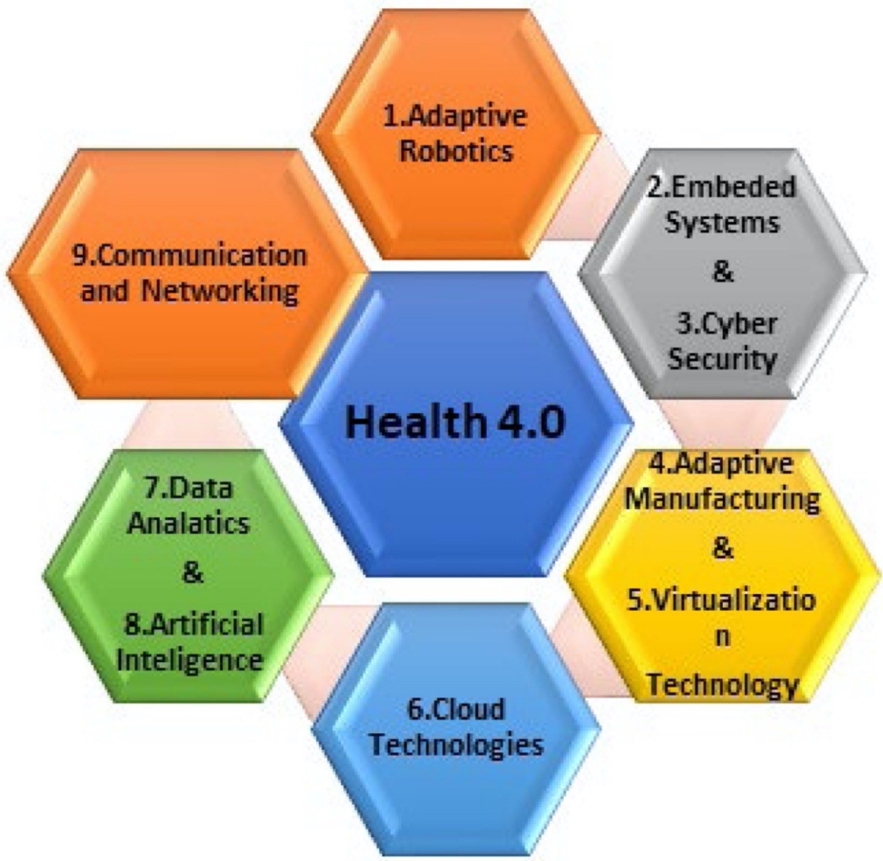

Fig. 2.1 Different categories of Health 4.0 (57)

enhancement of preoperative planning, surgical performance, therapeutic support, or training, to improve outcomes and reduce harm" (58). Digital surgery exploits real-time analytics with technology (59). As shown in Fig. 2.2, the components of digital surgery can be categorized into three key areas: data, analysis, and applications. Data is central both to the development and use of digital surgical technologies. Digital surgery not only involves the use of digital technology during surgery, but also encompasses a transformation in the culture and practice of surgery. Traditionally, the focus of surgery has been on postoperative outcomes, with minimal attention given to collecting data within the operating room. AI, computer vision and ML systems are proving that today the machines analyze large amounts of data faster and better than human beings (60). AI is an integral part of digital surgery (58,61). The adoption of AI and the generation of large amounts of data raise important ethical and legal concerns that should not be overlooked (62).

In the next sections, the role of AI as a support for surgeons will be investigated, with a focus on the application of AI in bowel perfusion assessment during colorectal surgery.

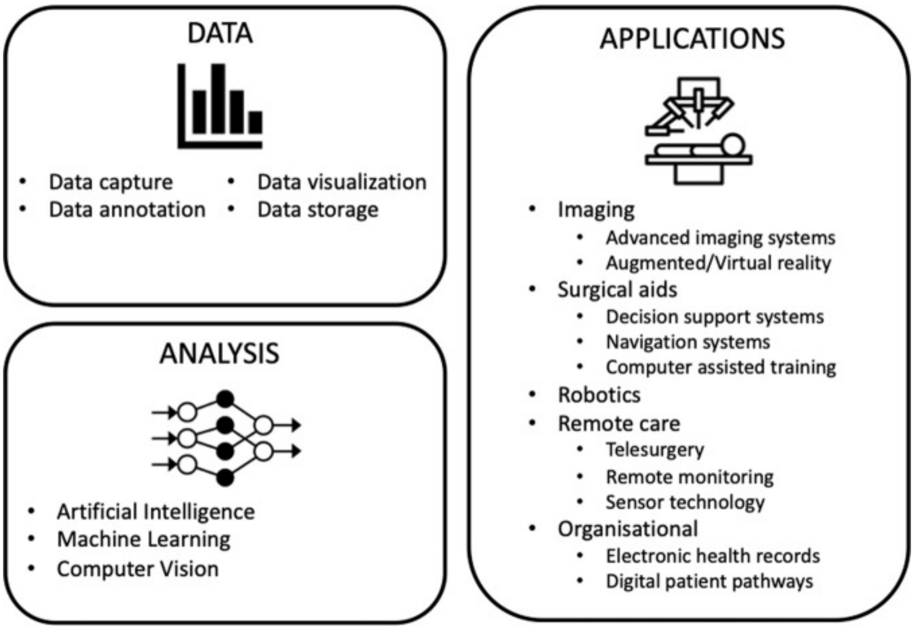

Fig. 2.2 Elements of digital surgery (58)

2.1 Artificial intelligence in the surgical field

Artificial intelligence (AI) can be defined as the ability of a digital computer or computer-controlled robot to perform tasks commonly associated with intelligent beings (63). It refers to computer systems that are designed to think or act like humans (human approach) and systems that think or act rationally (rational approach). A rational agent is one that acts so as to achieve the best outcome or, when there is uncertainty, the best expected outcome (64). AI encompassing multiple technologies, which can be divided into two main categories: data-driven AI and knowledge-based AI. Data-driven AI leverages large datasets to train models for predictions and decisions. It relies on techniques like neural networks and statistical learning. These techniques are commonly employed in applications with abundant data, such as image and speech recognition, natural language processing, and predictive analytics. On the other hand, knowledge-driven AI uses a formal representation of knowledge to make decisions and inferences using reasoning and logic and is typically used in applications where data is limited, such as expert systems, decision-support systems, and natural language understanding (61).

In general, AI applications in the medical field have two main branches: virtual and physical. ML and deep learning (DL) constitute the virtual component of AI (65). Figure 2.3 shows the fundamental relationship between AI, ML, and DL.

ML refers to a set of techniques that enable systems to learn from available data (training) and, through generalizing the training experience, analyze new data and make predictions within the same application domain as the training data. In 1959, the American scientist Arthur Samuel described ML as the "field of study that gives computers the ability to learn without being explicitly programmed". More recently, Tom Michael Mitchell, director of the ML department at the Carnegie Mellon University, provided a widely quoted, more formal definition of ML algorithms: "A computer program is said to learn from experience E with respect to some class of tasks T and performance measure P, if its performance at tasks in T, as measured by P, improves

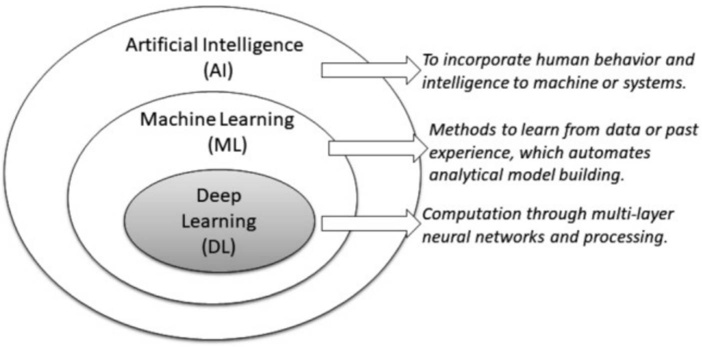

Fig. 2.3 Relationship between AI, ML, and DL.

with experience E." Experience exists in the form of training datasets, which aid in achieving accurate results on new and unseen data (66).

With the advancement of big data and increased computational capabilities, the field of DL has grown significantly. In 2006 the concept of DL was introduced by Hinton et al. in their article "A fast learning algorithm for deep belief nets" (67). DL is a branch of ML based on the concept of artificial neural networks (ANNs), which are collections of connected artificial neurons inspired by biological neural networks. ANNs typically consist of an input and output layer with one or multiple hidden layers within. Each neuron generates a series of real-valued activations for the target outcome. Like ML, DL also represents learning methods from data, where the computation is done through multi-layer neural networks and processing. The term "deep" refers to the concept of multiple levels or stages through which data is processed for building a data-driven model. DL differs from standard ML in terms of efficiency as the volume of data increases. DL modeling is highly beneficial when working with a large volume of data due to its ability to process a wide range of features and create a powerful data-driven model (68).

ML algorithms are classified into supervised, unsupervised and reinforcement learning. Supervised learning refers to learning techniques that infer the underlying relationship between the observed data (also called input data) and a target variable (a dependent variable or label). These techniques use a training dataset to develop a prediction model by consuming input data and output values. The model can then make predictions of the output values for a new dataset. Two main types of supervised learning are: classification, which entails the prediction of a class label, and regression, which entails the prediction of a numerical value. Unsupervised learning algorithms are designed to discover hidden structures in unlabeled datasets, in which the desired output is unknown. The general approach to learning involves training using probabilistic data models. Two popular examples of unsupervised learning are clustering and dimensionality reduction. Reinforcement learning involves exploration of an adaptive sequence of actions or behaviors by an intelligent agent in a given environment with a motivation to maximize the cumulative reward. The intelligent agent's action triggers an observable change in the state of the environment. This methodology can be seen as a trial-and-error learning paradigm with rewards and punishments associated with a sequence of actions (66).

The second form of application of AI in the medical field includes physical objects, medical devices, and increasingly sophisticated robots (65,69). However, it should be emphasized that the da Vinci® system, currently used in robotic surgery, is a master-slave system or tele-manipulator. It is not an autonomous system with the "ability to perform intended tasks based on current state and sensing without human intervention", according to the definition of the International Standard Organization (70).

Surgery is in its fourth generation (open surgery, endoluminal surgery, laparoscopic surgery, and robot-assisted surgery). Minimally invasive surgery provides a huge amount of data which can be processed by AI. However, analyzing images in minimal access surgery can be a challenge due to various factors such as changes in illumination, unfocused frames, presence of blood and smoke in the surgical field, and anatomical diversity. In addition to data from videos, robot-assisted surgery also generates data from robot kinematics and events, such as pressing camera buttons and clutching pedals (71). Given this large amount of data, the field of Surgical Data Science (SDS) is actively growing. It aims to improve the quality of interventional healthcare by collecting, organizing, analyzing, and modeling data (72).

Surgical video analysis is one of the most common applications of AI in surgery. A schematic representation is depicted in Fig. 2.4. Once a clinical need has been clearly defined, the next step is to generate an appropriate dataset that is large-scale and representative. To ensure the suitability of the data, it is recommended to check if subject-matter surgeons regularly use and successfully address the identified problem using this specific type of data. The agreement among experts can also give an idea of how much data are needed to train and test an AI model.

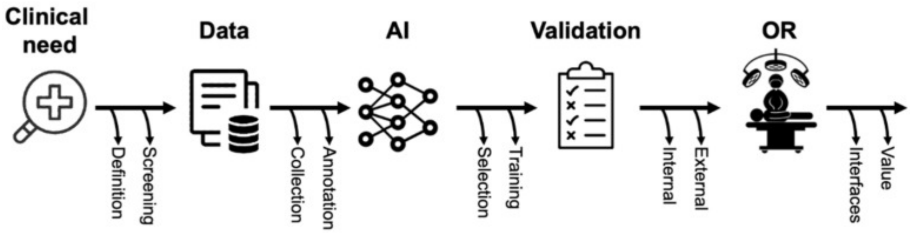

Fig. 2.4 Typical AI pipeline in the surgical field (73)

When experts have lower agreement, it usually means that larger datasets are needed to solve more complex problems. A further step in generating a dataset for AI is annotation, which describes the process of labeling data with the information the AI should learn to predict. High-quality annotations are essential for training AI using supervised learning approaches. The annotated dataset should be divided into a training set, which will be used to develop the AI algorithm through multiple iterations, and a test set, which will be used to evaluate the AI's performance on unseen data. Test data should not be exposed during training and should remain as independent as possible from the training dataset. At this stage, the dataset and task of interest will be explored to select the best AI architecture or algorithm to then refine, train, and test. In most cases, healthcare professionals and computer scientists collaborate in this process. Interdisciplinary education is crucial in order to allow all stakeholders to comprehend both the clinical and algorithmic perspectives, evaluate relevant literature, and promote effective interdisciplinary collaboration. Then, external validation and translational studies are essential to evaluate the clinical potential of the AI system. Since the performance of AI is significantly influenced by the training data, it is important to test AI systems on data from multiple centers that represent different acquisition methods, patient populations, and hospital environments. This enables the evaluation of how well AI systems can generalize beyond the development setting. However, very few external validations studies have been performed to date. Finally, research on integrating this technology into complex clinical and surgical workflows, and evaluating how these changes affect patient care, is crucial for measuring the real value for patients and healthcare systems (73).

Surgical procedures require a combination of situational awareness, decision-making abilities, technical skills, as well as cognitive and procedural competency in order to be successful. At the forefront of research, there are numerous instances of ML-based approaches being utilized in the field of surgery. These approaches have the potential to improve the aforementioned aspects. AI can be used in surgery to assist with intraoperative navigation and to identify and prevent errors early. The development of AI-based context-aware systems can greatly enhance decision-making, which is one of the most challenging tasks in surgical practice. This improvement can lead to reduced risks for patients, prevention of complications, and overall enhancement in healthcare services. AI applications can also be used to assess surgical skills objectively during training, to automate surgery using the concept of self-driving cars in robot-assisted surgery as well as for diagnostic purposes and optimization of perioperative care (61,71,73).

While other areas of surgery, like orthopedics, neurosurgery, and maxillofacial surgery, have already adopted surgical planning using computer-generated models and intraoperative navigational aids, the use of AI methods in gastrointestinal surgery, especially colorectal procedures, is still in its infancy. No AI algorithm has been approved for clinical use to date (59,73,74).

2.2 Applications of artificial intelligence in colorectal surgery

As for other fields of surgery, colorectal surgical outcomes great rely on the efficacy of intraoperative decisions and actions as well as on the accuracy of preoperative assessment and the adequacy of postoperative care. Although still in their early stages, artificial intelligence (AI) applications have been explored in all the phases of the surgical pathway (61).

Critical aspects of the preoperative phase include choosing the ideal treatment, assessing the risk for perioperative complications and poor outcomes, optimizing patient clinical condition, and creating tailored treatment pathways for each patient. Clustering algorithms based on clinical data have been used for prediction of cancer stage, which informs the treatment plan (75). Unsupervised ML has been useful in identifying and monitoring care pathways that have shown favorable performance in terms of shorter hospital stay, fewer 30-day readmissions, and lower costs (76). ANNs have been utilized to predict the interval between diagnosis and surgery, in order to customize patient preoperative optimization. This prediction achieved an accuracy of 90% (77). The value of AI supporting systems like IBM's Watson for Oncology (WFO) in the clinical decision-making process for colorectal cancer treatment has been explored. Aikemu et al. investigated the concordance between treatment recommendations for colorectal cancer patients given by WFO and a multidisciplinary cancer team. The concordances for colon cancer, rectal cancer, or overall were all 91% (78). Other AI tools are designed for preoperative risk assessment. Azimi et al. developed some prediction models using preoperative features to identify those patients at higher risk of postoperative infections after colectomy. This can help clinicians better control the modifiable factors that are known from the literature to be significantly associated with postoperative infectious complications. Naïve Bayes and Support Vector Machine had the best performance with an area under the curve (AUC) of 0.81 (79). Similarly, Sammour et al. developed an online calculator (http://www.anastomoticleak.com) to predict the risk of AL after colon cancer resection. The calculator was based on the ANACO study group nomogram and included six independent variables (gender, body mass index, oral anticoagulants, intraoperative complication, serum protein level, hospital size). The authors utilized IBM Watson Analytics to analyze an anonymized dataset and identify a predictive model. Among all the variables evaluated by the AI software, the calculator output and patient age were identified as independent predictors of leak. Modification to the online calculator because of the analytics slightly improved its performance (80,81). ANNs have also been employed to predict delayed discharge and readmission following laparoscopic colorectal cancer surgery (82). Finally, various radiomic models have been used on preoperative magnetic resonance or computed tomography images to predict the response to preoperative chemoradiation in patients with rectal cancer (83), nodal or liver metastases (84,85), and gene mutations (86).

Intraoperatively, AI assistance has primarily focused on minimally invasive surgeries, which natively rely on the use of endoscopic video to guide such procedures (73). AI has primarily been proposed for identifying surgical phases or tracking devices, as well as distinguishing tumor tissue from normal bowel wall. Kitaguchi et al. established the LapSig300 dataset which includes 300 laparoscopic colorectal surgery videos from 19 high-volume Japanese centers. More than 82 million frames from the videos were labeled with the surgical phase and action under the supervision of two colorectal surgeons, while more than 4000 images were labeled with tool annotations and the tool area was extracted for a segmentation task. A convolutional neural network was used to analyze the videos. The accuracy rates for automatically classifying surgical phases and actions were 81.0% and 83.2%, respectively. However, further improvement is needed when it comes to recognizing surgical tools (87). In an *in-vivo* study, Baltussen et al. evaluated the accuracy of diffuse reflectance spectroscopy for tissue characterization during colorectal cancer surgery. Using two Support Vector Machines, the classification resulted in a mean accuracy for fat, healthy colorectal wall, and tumor of 0.92, 0.89 and 0.95 respectively (88). Integration of AI into robotic platforms has also been attempted. The Smart Tissue Autonomous Robot (STAR) system, developed at the Johns Hopkins University, could autonomously complete bowel anastomoses in both ex-vivo and in-vivo animal models with equal or better performance than its human counterpart (89). Initial experiences of AI-enhanced surgery using ICG applications will be discussed in the section 2.4.

In the postoperative phase, ML algorithms and ANNs have mainly been proposed as early warning systems for complications (90,91). DL models have also been used to provide recommendations about postoperative chemotherapy (92). Moreover, voice recognition technologies have been employed to monitor patients in the post-discharge setting (93).

Additional areas of AI applications include the assessment of patient-reported outcomes, automated pathology assessment, and research (61). An overview of potential applications of AI in colorectal surgery is provided in Figure 2.5.

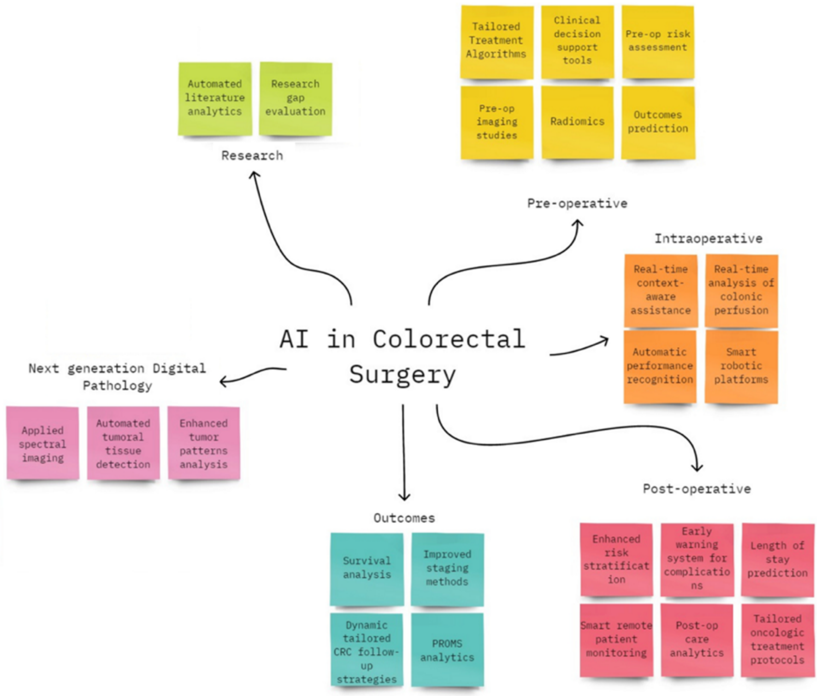

Fig. 2.5 Fields of application of artificial intelligence in colorectal surgery (61)

2.3 Quantitative indocyanine green fluorescence angiography

In the previous chapter, we discussed the limitations of indocyanine green fluorescence angiography (ICG-FA), specifically its susceptibility to individual interpretation. Hence, an objective (quantitative) methodology is needed to overcome the inherited observer bias. Different from visual ICG-FA, where the surgeon assesses the fluorescence signal, quantitative ICG-FA (Q-ICG) involves an algorithm that interprets the fluorescence signal. This is translated into a fluorescence-time curve. Subsequently, the system can calculate different parameters, which reflect the perfusion of the examined tissue (94).

Briefly, the NIR camera is placed at a set angle and distance to the target tissue. Regions of interest (ROIs) are selected by the surgeon under white light. The ICG-FA system is activated and ICG is injected intravenously. The Q-ICG software generates a fluorescence-time curve based on the average pixel intensity of a selected region of interest (ROI) and plotted against time. The fluorescence-time curve has different phases as depicted in Figure 2.6. During ICG administration, the curve displays baseline static. In the next phase, ICG molecules enter the target tissue and, excited by the NIR light, begin to

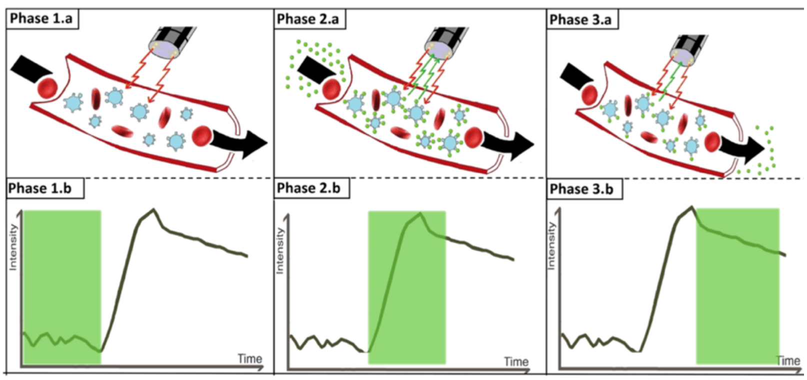

Fig. 2.6 A schematic overview of the different Q-ICG phases (95)

emit fluorescence. A steep increase in fluorescence intensity is observed in the curve. This is the inflow phase. Finally, ICG is removed by hepatic clearance, and the curve displays a steady decline in fluorescence intensity. After generating the fluorescence-time curve, the Q-ICG software calculates Q-ICG parameters from the ROI selected by the surgeon. A visual representation of the various parameters is given in Figure 2.7. Relative parameters can also be obtained by selecting two ROIs. The reference ROI is placed within an area with excellent perfusion, while the target ROI is placed in an area at risk of reduced perfusion. The relative parameters are obtained by dividing the target ROI with the reference ROI.

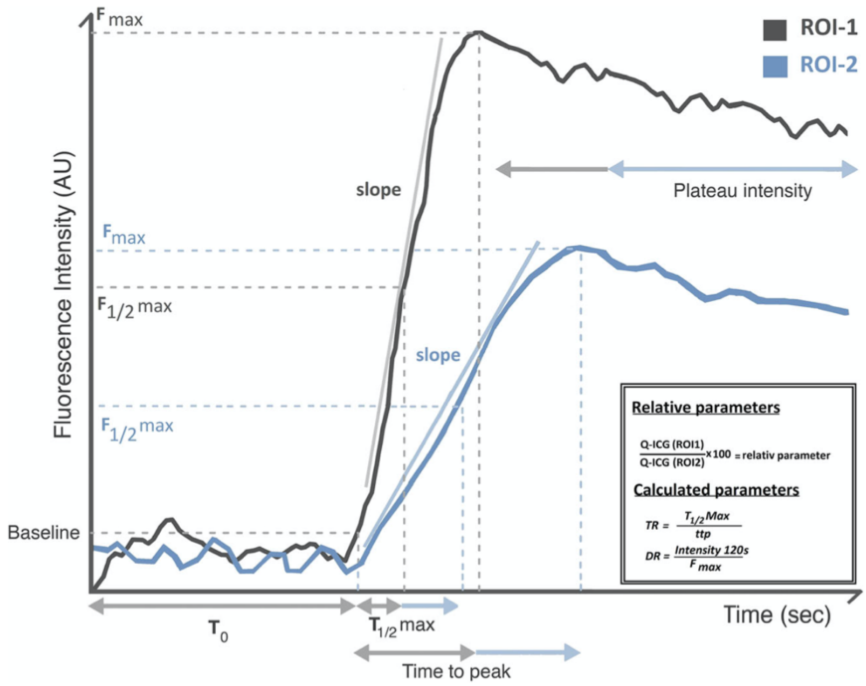

Fig. 2.7 Q-ICG. A visual representation of the fluorescence-time curve and its different parameters (95)

Q-ICG parameters can be divided into two categories: inflow and intensity parameters. The former are defined from the timing of distinct perfusion events, while the latter are based on absolute fluorescence measurements. Inflow parameters include the following: time-to-peak (*ttp*): the time to reach the maximum fluorescence intensity (F_{max}); slope (*slp*): the differential to the fluorescence-time curve during the *ttp* interval; $T_{1/2max}$: the time from the first intensity increase until 50% of maximum intensity is reached; T_0: the time to first fluorescence signal. Intensity parameters include the following: the maximum fluorescence intensity (F_{max}); drainage ratio (*DR*): the absolute intensity value at 120 s divided by F_{max}; plateau intensity (*PI*): the median value intensity in the last 25% of the ICG-FA (95).

Several factors may distort the validity of the Q-ICG readings, including camera distance and angulation, camera movement artifacts, light reflections at the bowel wall, and movement of the target ROI. The fluorescence intensity decreases with increased camera distance due to the inverse-square law. Also, with increased angulation to the target ROI, less light illuminates the tissue and the lens (96,97). Moreover, the varying anatomy of patients' microcirculation leads to significant interindividual differences in ICG quantitative parameters. These are affected by ICG plasma concentration, systemic perfusion factors (cardiac output, blood pressure, vasoconstrition), overtime retrograde flow of ICG within tissues (95).

Q-ICG is still a novel technology, and currently, no Q-ICG parameter or methodology is considered a gold standard. Q-ICG parameters have mostly been examined in animal models (98,99) and a few clinical studies have been conducted, where Q-ICG analysis was commonly performed post-hoc by analyzing video recordings of the ICG-FA. The animal studies found that both inflow and intensity Q-ICG parameters do correlate with visceral perfusion given the controlled experimental conditions. However, in the clinical setting, the inflow parameters (especially *slp* and $T_{1/2max}$) perform better and exhibit a stronger correlation with AL than intensity parameters. This is because inflow parameters, which rely on the timing of perfusion events rather than the numerical intensity values, are less affected by the environmental, tissue, and patient factors mentioned above. These, instead, strongly influence intensity factors.

Currently, many different software systems for Q-ICG are available, and a small number of commercial ICG-FA systems offer built-in support for intraoperative Q-ICG (although only employing intensity parameters). However, one major limitation of Q-ICG is interpreting measurements. Q-ICG still lacks verified procedure-specific cut-off values for swift objective decision-making in the operating room. Only a few studies (100–102) have suggested cut-off values for AL based on *slp*, $T_{1/2\max}$, $F_{\max}$, and *ttp*, but these values are not validated. As a matter of fact, although Q-ICG provides objective measurements, clinical decisions will remain subjective unless cut-off values are established.

2.4 Artificial intelligence analysis for indocyanine green fluorescence

In the field of fluorescence imaging for intraoperative guidance, early reports have investigated the role of ML for cancer tissue discrimination, characterization of liver metastases, and bowel perfusion assessment.

Cahill et al. developed a computer vision real-time tissue-tracking and categorizing prototype (103). Intraoperative videos captured using white-light and NIR fluorescence imaging techniques were utilized for both training and testing the AI model. These videos displayed colorectal tumors, both benign and malignant, along with the surrounding normal tissue. Following video capture and tissue annotation by the surgical team, a number of ROIs were chosen from each surgical field of view. A custom video-tracking algorithm was used to adjust external factors while gathering time-varying pixel intensities that represented ICG brightness within the ROIs across consecutive video frames. The extracted NIR intensity data were then fitted to a parametric curve derived from a biophysical model, which was created to capture both the inflow behavior and exponential decay of the ICG bolus. A supervised method was used to train ML-based classification models on a library of archival videos for cases with known pathology results to differentiate healthy tissue from tumor within each ROI. After training, the model proceeds to assign the pathology label to unseen cases based on the assumption that patterns hold more broadly. The mean accuracy was 86.4%. Notably, the model was applied in two patients intraprocedurally, providing real-time data acquisition, AI analysis, and tissue classification within 10 minutes.

Hardy et al. used ML to demonstrate and characterize colorectal liver metastases following intraoperative ICG administration (104). Video recordings of 25 consenting patients with liver lesions undergoing surgery were analyzed. User-selected ROI perfusion profiles were generated, milestones relating to ICG inflow/outflow extracted and used to train a ML classifier. This classified 97.2 % of liver metastasis ROIs within 90 s of ICG administration following initial mathematical curve analysis identifying ICG inflow/outflow differentials between healthy liver and metastases.

Park et al. explored the usability of a ML algorithm for assessment of bowel perfusion (105). The ICG curves were obtained from 200 ROIs across 65 videos of laparoscopic colorectal surgery. Curves were preprocessed to decrease the degradation of the AI model due to external factors. The authors employed unsupervised learning to cluster 10,000 ICG curves into 25 patterns with a self-organizing map (SOM) network. The training was performed using the neural net clustering in MATLAB 2019 (MathWorks, Natick, MA, United States). Subsequently, anastomotic risk labelling was performed for each classified pattern using a simplified colorectal vessel model and colonic circulation simulator and data on patient complications. When new ICG curves from additional videos were used for testing, the learned network classified it into the most similar pattern and evaluated risk. A color mapping system that classifies the level of vascularization in red-green-blue areas was created. Based on comparing the AUC of the AI-based method with $T_{1/2\max}$, time ratio ($T_{1/2\max}/T_{\max}$), and slope, the AI model demonstrated a higher accuracy in the perfusion assessment, with values of 0.842, 0.750, 0.734, and 0.677, respectively.

Chapter 3

Proposal and implementation

The fluorescence imaging technology has shown itself to be a useful intraoperative predictive test for evaluating perfusion during colorectal resections. However, as discussed in the previous chapters, the use of ICG-FA relies on the subjective interpretation of the results by the surgeon. Even though systems for Q-ICG provide a graphical output, surgeons still have to interpret it subjectively.

In the field of surgical research, ML is playing an increasing role to address the issue of subjectivity and provide real-time support for operators. This helps minimize risks for patients, prevent complications, and enhance outcomes, particularly when less experienced operators are involved in the care pathway.

The research activity conducted in this doctorate explored the feasibility of a ML-based system to gather information on bowel perfusion from ICG-FA videos recorded during minimally invasive colorectal surgeries. The objective is to create a decision-support system that can automatically evaluate the quality of perfusion. Such a system can inform the surgical strategy to minimize the risk of AL, which negatively impacts on patients, surgeons, and healthcare system.

3.1 Overview of the research activity

During the research activity, three main tasks for the ML application were identified: evaluating bowel perfusion based on fluorescence intensity, identifying the optimal bowel transection line based on fluorescence intensity, and assessing bowel perfusion based on the temporal trend of fluorescence diffusion.

3.1.1 Evaluation of bowel perfusion based on fluorescence intensity

The aim was to create a system that automatically assesses the amount of ICG in a ROI chosen by the surgeon and then provides an output classifying bowel perfusion as either adequate or inadequate. This issue can be formally expressed as a two-class classification problem.

For this purpose, colorectal laparoscopic surgeries were recorded as movie files. Videos showing the bowel to be anastomosed after injection of ICG were directly acquired from the endoscope during the procedures and collected. In each video, the surgeon selected a ROI as a rectangular box using the mouse or trackpad on the computer when initiating the algorithm. The frames coming from the video streaming and the selected ROI were the input of the system. The overall architecture of the systems entails three main blocks (Fig 3.1).

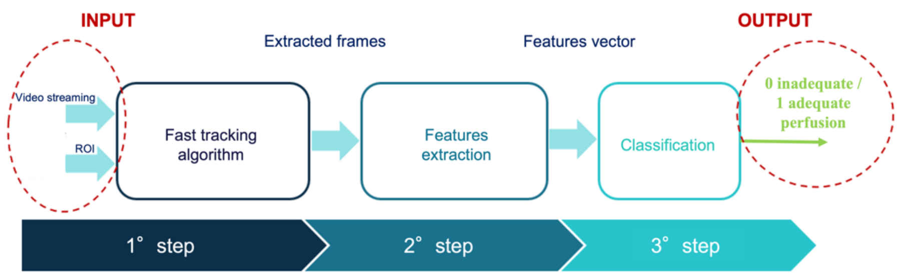

Fig. 3.1 Block architecture of the proposed algorithm

The first one is a fast-tracking algorithm, which is used to track the selected ROI during the video execution. Once the frames containing the ROI are extracted from the video source, the second block performs a features extraction. The ROI of each frame is divided into 20 vertical equal slices and, for each of them, the histogram of the green band and its area is computed. Figure 3.2 illustrates the overall process of features extraction. The area of the histogram constitutes an element of the

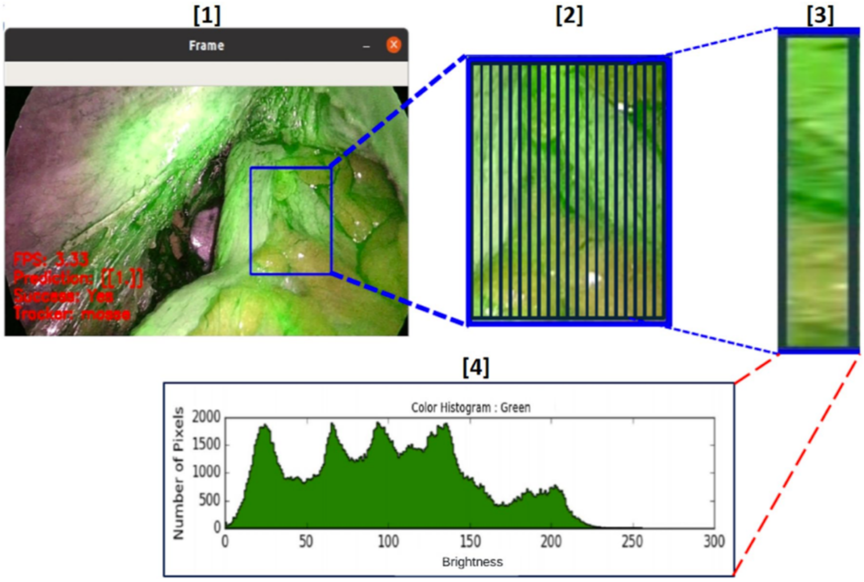

Fig. 3.2 Features extraction. 1) ROI selection. 2) The ROI is divided in 20 slices. 3) For each slice, the histogram of the green band is evaluated. 4) The amount of green of each histogram is evaluated and the obtained feature is used to build the feature vector sent to the ML classifier (106)

feature vector. Thus, a vector of 20 elements is obtained and becomes the input to the last functional block. This step of the process binarily classifies the feature vector and establishes whether it corresponds to adequate/1 or to inadequate/0 perfusion of the colonic stump to be anastomosed. This classifier is obtained by a Feed Forward Neural Network. During the laboratory experimental validation, a dataset of 11 videos of laparoscopic left-sided colorectal resections collected and labelled by surgeons was used to train and validate the ML classifiers. The preliminary obtained results show a classification accuracy equal to 99.9%, with a repeatability of 1.9%. Finally, the real-time operation of the proposed algorithm was successfully tested by analyzing the video streaming captured directly from an endoscope available in the operating room. Future work may address introducing more levels between adequate and inadequate perfusion, identifying a method to automatically select the ROIs, and enrich the dataset by facing circumstances when the blood perfusion is impaired by underlying diseases (106).

3.1.2 Identification of the optimal bowel transection line

The aim was to create an automated system that helps surgeons determine where to divide the bowel before performing an anastomosis. Thus, the algorithm presented earlier has been further developed to provide the optimal bowel transection line as the output. Similar to the previous one, the ROI of each frame is divided into 20 vertical equal slices. The histogram of the green band for each slice and its area is computed (Fig. 3.3).

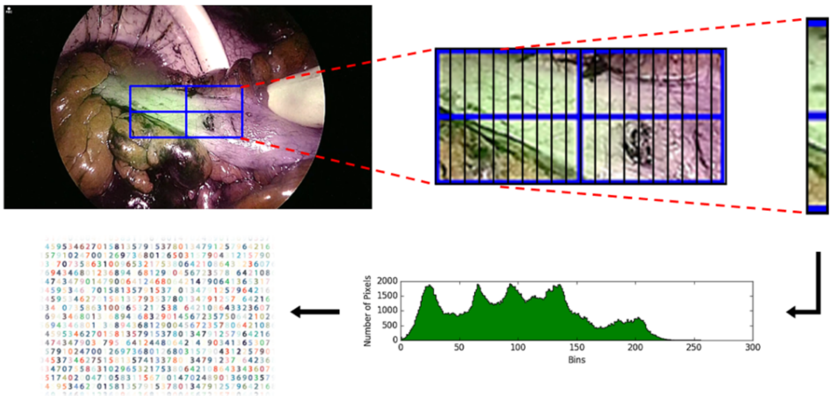

Fig. 3.3 ROI selection and feature extraction

Each frame is analyzed, and a matrix is created in which the columns represent the slice and the rows the analyzed frame. The matrix indicates the green change over time and represents the input of a Feed Forward Neural Network. The network assigns a probability to each slice, indicating the likelihood that it is the best slice for cutting. The final prediction corresponds to the highest probability value. The prediction is displayed on the video as a red line at the chosen slice. The transection line is predicted in real time, so it can change whenever the video changes. A steady state message appears when the prediction is stable (Fig. 3.4).

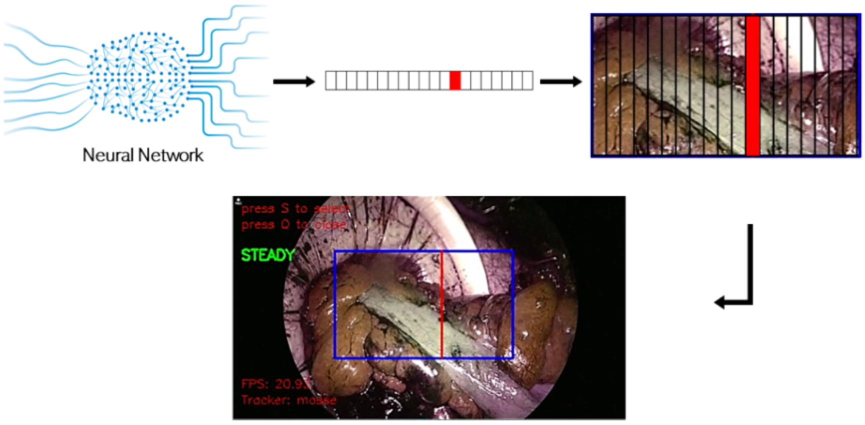

Fig. 3.4 Prediction of the optimal transection line

The obtained results show a classification accuracy equal to 82.7%, with a repeatability of 3.23% (unpublished data). Even for this system, the real-time operation of the proposed algorithm was successfully tested in the operating room.

3.1.3 Evaluation of bowel perfusion on the temporal trend of fluorescence diffusion

Based on the hypothesis that the timing of fluorescence shows a stronger correlation with postoperative complications, a more complex issue was addressed. This is the assessment of perfusion based on the temporal trend of ICG fluorescence diffusion. As described in section 2.3, the fluorescence signal can be translated into a fluorescence-time curve with different phases (baseline, inflow, and plateau) corresponding to the events that occur on a capillary level during the FA-ICG (Figures 2.6 and 2.7). From this curve, several intensity parameters and inflow parameters can be calculated, which provide information about tissue perfusion. Indeed, based on the most recent data from the literature, it seems that inflow parameters may be more resilient to the different environmental and patient factors that can impact ICG perfusion assessment, as compared to the intensity parameters. Also, the inflow parameters may be more effective in predicting the risk of AL. Thus, the final objective is to create a ML system that automatically assess the quality of bowel perfusion based on the fluorescence-time curves. The initial step in this process, which represent the core of this thesis, is to develop an unsupervised learning method (clustering) that groups the fluorescence intensity-time curves based on their similarity. Thus, patterns of ICG curves can be obtained. The subsequent step will be to develop an ICG curve pattern classification model to establish whether a ROI is adequately or inadequately perfused.

3.2 Dataset

Although laparoscopic and robotic cameras can be used to capture still images or videos, it can be challenging to gather high-quality data during a surgical operation due to various constraints. Recording proper surgical videos for experimental purposes can disrupt the regular flow of surgical phases and actions, potentially leading to an increased mental effort for the surgical team, longer duration of the procedure and, potentially, to patient safety issues. This because surgical decision-making is unique, requiring quick actions which are highly contextual (58). Moreover, authorization is required to guarantee patient's privacy.

The videos used for this work were collected by the medical staff of two general surgery units at the University Hospital Federico II of Naples and Santa Maria delle Grazie Hospital of Pozzuoli. Videos were recorded during both laparoscopic and robotic colorectal surgeries, including left colectomy and anterior rectal resection. In detail, after ligating the major blood vessels, fully mobilizing the left colon, and transecting the rectum, the surgical specimen was extracted through a suprapubic incision. After dividing the mesocolon and marginal artery at an appropriate line for transection of the descending colon, a 5 mg/ml

ICG solution was administered intravenously by bolus injection followed by a saline flush (10 mL). A body-mass adjusted dose of 0.25 mg/kg was injected through an 18-gauge peripheral catheter placed in the forearm. The blood flow in the proximal colon was evaluated by a NIR camera system, namely the da Vinci Xi 30° Endoscope Plus with Standard Firefly Mode for robot-assisted surgery and Olympus CH-S200 camera with 30°, 10-mm IR telescope for laparoscopic surgery. The camera was fixed 15 cm apart from the extracted specimen and lights of the operating room were completely turned off. The bowel was filmed starting before the injection of ICG, which was indicated by a thumbs up in the video.

ICG videos were discarded if they showed any significant interference during angiography recording, such as passing of hands and/or surgical instrumentation over the ROI, or too abrupt camera movements.

The final dataset consisted of ICG videos collected from 27 patients. Files were in the ".mp4" format at a rate of 30 frames per second.

3.3 Methods

The aim is to provide a method that, by randomly choosing a sufficient number of ROIs from the picture, generates intensity-time curves of the green light in each ROI for subsequent clustering. The proposed algorithm starts with the acquisition of ICG-FA videos recorded during colorectal surgeries. Videos are pre-processed and standardized and then a number of ROIs are placed randomly throughout the first video frame. After using a tracking algorithm, the information on the green fluorescence light intensity over time is collected and given as input to two ML algorithms for clustering. The architecture of the proposed system is shown in Fig. 3.5.

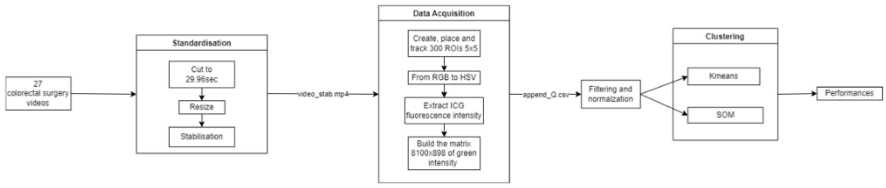

Fig. 3.5 Block architecture of the proposed algorithm

3.3.1 Pre-processing

A pre-processing phase is needed to have consistent data. To ensure that all videos were of the same length, an editing program was utilized to crop the recordings. In most cases, the fluorescent emission began approximately 5 seconds after the surgeon's signal on the video and reached its peak at around 25 seconds. Thus, it was decided to cut the videos at 29.96 s, for a total of 898 frames from each video.

The pre-processing phase included video resizing and stabilization. A video resizing was performed to decrease the size of the input recordings. This enables to work with smaller files in the next phase and reduce the execution time. Stabilization aims to transform a recording that has been affected by unintentional camera movements into a stabilized version where these movements are smoothed out. This operation can significantly reduce video image movement, but it cannot eliminate it entirely.

3.3.2 Fluorescence-time curve acquisition

Once the videos were ready to be analyzed, the data acquisition process was started. The idea was to select a substantial number of ROIs to collect valuable data without impeding performance. Information on the mean fluorescence intensity is taken from the ROIs. Fluorescent color extraction was conducted after converting the RGB (red, green blue) color space into the HSV (hue, saturation, value) color space. This makes the algorithm less sensitive to image lightness and enables to remove distortion-producing factors such as background and light source reflection.

Three-hundred ROIs, each consisting of a 5x5 pixel square window, were automatically generated and randomly positioned on the first video frame. Thanks to a tracking algorithm, the ROIs were tracked until the last frame. At the end of this process, the intensity of the green light over time was extracted, resulting in a fluorescence–time curve of 29.96 s seconds or 898 frames for each ROI. Since the dataset consisted of 27 videos, each containing 300 ROIs, a total of 8100 curves were extracted as a group on input data.

Fluorescence intensity–time curves were then processed using machine learning algorithms to extract the features necessary to determine the clusters.

3.3.3 Clustering

Two clustering algorithms were used: K-means and Self-Organizing Map. Clustering algorithms can be considered the leading methods of unsupervised learning. When the available data consists of unlabeled samples, or when each data point merely contains attributes without a label, unsupervised learning is a machine learning paradigm for solving the problem. It is also known as "class discovery" and is used to uncover useful patterns or structural properties of the data (107,108). Unsupervised learning aims to educate the machine learning algorithm to create a concise internal representation of the input through imitation, which is an important method of the human learning. Unsupervised learning is often performed as part of an exploratory data analysis. This approach significantly differs from supervised machine learning for the fact that there is no training set and, hence, no clear function for cross-validation. Since there is no universally accepted mechanism for performing cross-validation or validating results on an independent dataset, it can be hard to assess the results obtained from unsupervised learning methods (109).

Clustering refers to a set of techniques for findings subgroups, or clusters, in a dataset. When clustering a dataset, the goal is to separate the observations into distinct groups. The clustering algorithm distributes the data into the clusters according to their similarities. Within each cluster, the observations should be quite similar to each other, while the observations in different groups should be quite different. Grouping similar entities together will provide insight into the underlying patterns of distinct groups. Using a notion of distance between points and given a set of data points, these are grouped into several clusters, such that internal (intra-cluster) distances should be small, while external (inter-clusters) distances should be large (107). For clustering, a proximity measure for two data points needs to be defined, which means how similar or dissimilar the samples are with respect to each other. A measure usually used to indicate similarity/dissimilarity between two points is the Euclidean distance.

K-means

K-means is one of the most straightforward unsupervised learning techniques to address the clustering issue. The method has a minimal processing cost and uses a simple approach to partition a dataset of n observations into K distinct, non-overlapping clusters, with each observation belonging to the cluster with the nearest mean, serving as a prototype of the cluster. The means are commonly called the cluster centroids or cluster centers. K-means clustering minimizes within-cluster variation defined as the squared Euclidean distance. As a result, the data space is partitioned into K clusters (Fig. 3.6). To perform K-means clustering, the number of clusters is fixed *a priori*. The algorithm is iterative and consists of the following steps: 1) specifying a value for

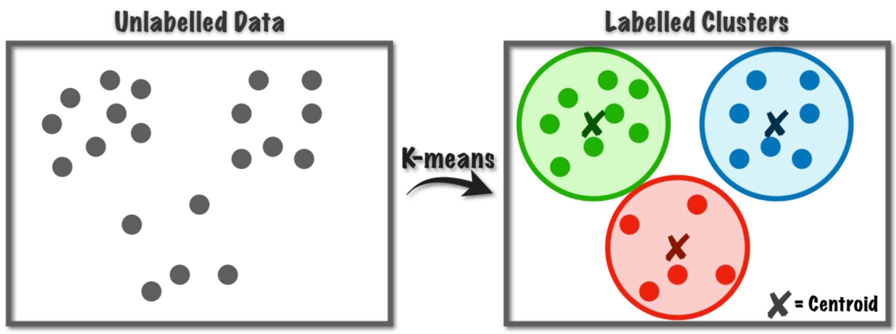

Fig. 3.6 K-means cluster algorithm operation

K and randomly choosing an initial centroid (center coordinates) for each cluster; 2) assigning all data points to the nearest centroids by using the Euclidean distance; 3) recalculating the cluster centers as a mean value of all the data points in each cluster; 4) reassigning the data points to the nearest clusters just recalculated. This process, assigning data points to the cluster centers and recalculating the cluster centers, is repeated until the cluster centers stop moving, and there is no further change in the clusters (110). At this point, the algorithm has converged, and the final clustering is retrieved (Fig. 3.7).

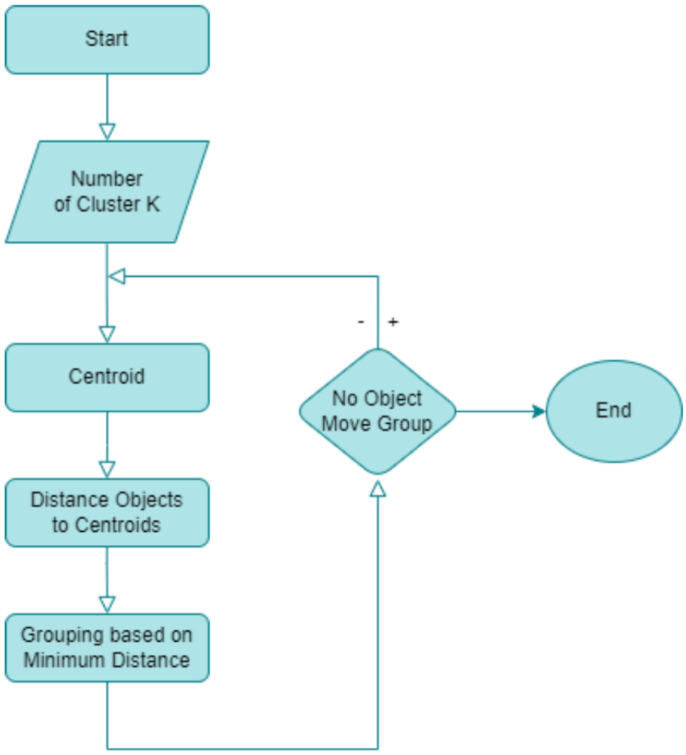

Fig. 3.7 Flowchart of the k-means clustering algorithm

Self-Organizing Map

Analyzing high-dimensional data can pose significant challenges due to the limitation of visualizing data in only two or three dimensions. A self-organizing map (SOM), which was invented by Kohonen in 1980, is a dimensionality reduction technique that can provide us with valuable insights about high dimensional data while requiring minimal computing resources. Self-Organizing Maps (SOMs) can be used for exploratory data analysis, clustering problems, and visualization of high dimensional datasets (111). SOMs are a type of artificial neural network that models the learning process of the visual cortex in the cerebral cortex and perform clustering by unsupervised learning (105). They create a low-dimensional representation of the input space, known as a "map". Map units or nodes typically create a two-dimensional space in such a way that some proximity measure is similar to the proximities in the original high-dimensional space. In particular, SOMs aim at preserving topology, that is, try to keep information on close neighbors (112). Two important layers compose SOMs: the input layer and the output layer, often known as a feature map (Fig. 3.8). Each node in the map space is associated with a weight vector with the same dimensionality as the input space (113).

Self-organizing maps, like most ANNs, operate in two modes: training and mapping. Training uses a collection of input data, or the input space, to generate the map space, while mapping classifies additional input data using the generated map. Training involves competitive learning, where the elements of an artificial neural network, in a sense, compete against each other for the chance to respond to the input, so that only one node can win at any given time. These nodes are known as winner-takes-all nodes. The Euclidean distance between the weight vectors and the input vectors is computed, and the winner node is determined by the minimum Euclidean distance. The weights of the winning node, as well as of its nearest neighbors are subsequently adjusted in order to move the weights closer to the input vector. The adjustment of the weights of the nodes near the winning node is instrumental for preserving the order of the input space. As a result, similar inputs are mapped to similar regions in the output space, while dissimilar inputs are mapped to different regions in the output space.

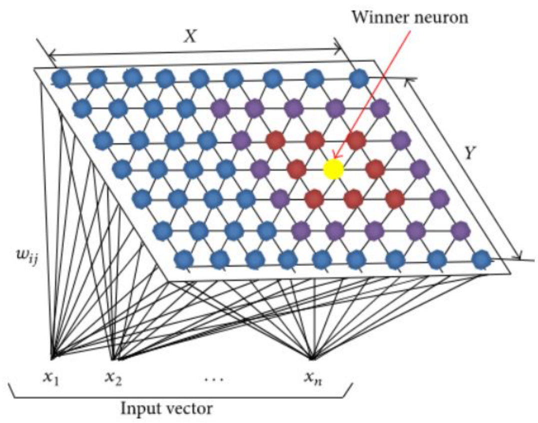

Fig. 3.8 SOM feature map. The yellow model represents the best match, and the surrounding models (shown in red) are its neighbors.

After updating the appropriate weights, the next iteration starts by presenting a new input vector to the updated nodes. With continued training, the size of the neighborhood decreases until the only node affected by the update is the winning node itself. The algorithm is complete when the positions of the nodes satisfy some predetermined condition of stability. A flowchart is shown in Fig. 3.9. After training, the map can be used to classify additional observations for the input space by finding the node with the closest weight vector, which corresponds to the smallest distance to the input space vector (113–115).

3.3.4 Validation of cluster consistency

The Silhouette was used to evaluate the performance of the clustering methods. Proposed by Rousseeuw in 1987, it defines for each object in dataset, the measure of how this object is similar to other objects from the same cluster (cohesion, compactness) in comparison with objects of other clusters (separation). For each object, the measure can have values ranging from -1 to 1. The higher value means better matching to cluster

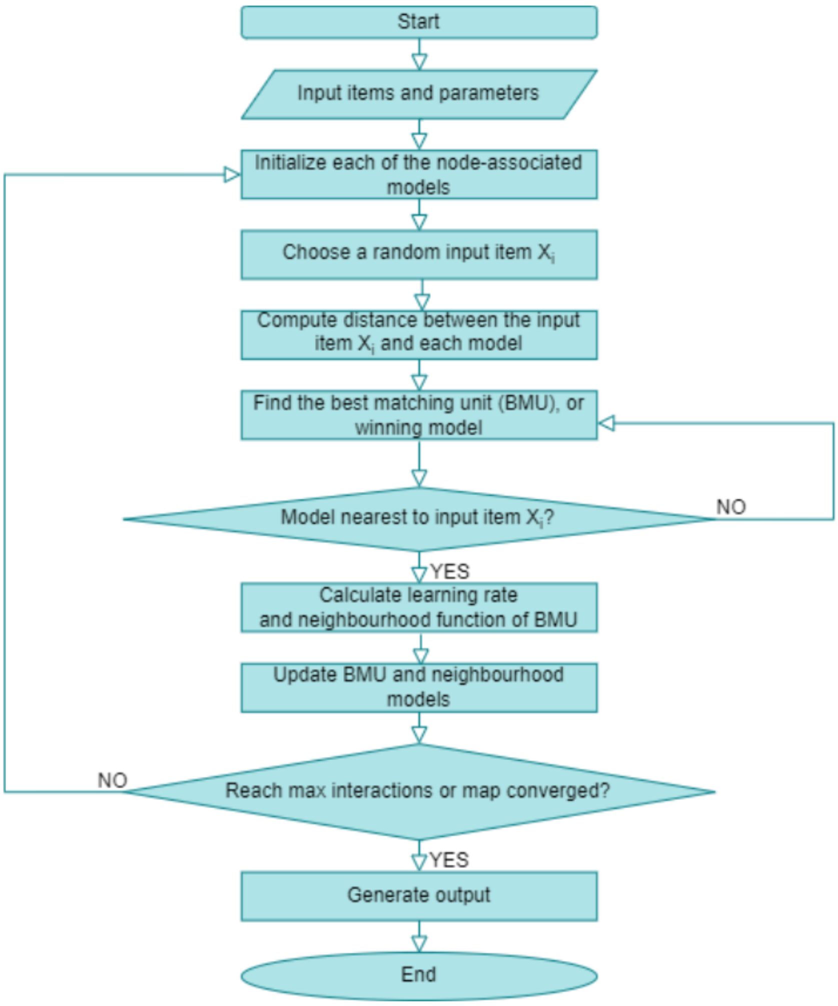

Fig. 3.9 Flowchart of the SOM algorithm

to which it should be classified and lower fitness to neighboring clusters (116). A value of 1 means the clusters are well apart from each other and are clearly distinguished, a value of 0 means the distance between clusters is not significant, and a value of −1 means clusters are assigned incorrectly (117). The Silhouette score is calculated using the mean intra-cluster distance and the mean nearest-cluster distance for each sample (Eq. 1).

$$S(u) = \frac{1}{n}\sum_{i=1}^{n}\frac{b(i) - a(i)}{\max\{a(i); b(i)\}}, \quad S(u) \in [-1, \ 1]$$

where

u—number of clusters,

n—number of objects in dataset,

$\{d_{ij}\}$—distance matrix,

$a\,(i) = \sum_{k\in\{P_r\backslash i\}} d_{ik}/\,(n_r - 1)$—average distance from object *i* to other objects belongings to cluster P_r (object *i* belongs to cluster P_r); n_r—number of objects in cluster P_r,

$b(i) = \underset{s\neq r}{min}\{d_{iP_s}\}$, $d_{iP_s} = \sum_{k\in P_s} d_{ik}/n_s$—average distance from object *i* to other objects belongings to cluster P_s (object *i* does not belong to cluster P_s); n_s—number of objects in cluster P_s.

Eq. 3.1. Silhouette score (116)

3.4 Implementation

The algorithm for this study was developed in Python 3.9 with the operating system Windows 11 Home version 22h2 from Microsoft. Python is a highly popular programming language worldwide, used extensively for web applications, software development, data science, and ML. It is a high-level language running on many different platforms and is free to download. By default, Python comes with a comprehensive standard library that includes a collection of commonly used codes. In addition, a sizable number of Python libraries are available for various applications (118). The most popular libraries used for this work include Matplotlib, NumPy, OpenCV, and Scikit-Learn. Matplotlib is used to plot data in high-quality two- and three-dimensional graphics. NumPy, short for Numerical Python, is used to efficiently create and manage arrays and perform linear algebra operations. It enables faster work with matrices and vectors. OpenCV (Open-Source Computer Vision Library) is an open-source library for computer vision, machine learning, and image processing. More than 2,500 optimized algorithms are available in the collection, which can be used for a large number of tasks, such as detecting and recognizing faces, identifying objects, classifying human actions in videos, tracking camera movements and moving objects, recognizing scenery and establishing markers to overlay it with augmented reality. Scikit-Learn or Sklearn is the most useful and robust library for machine learning in Python. It is largely written in Python and is built upon NumPy, SciPy (which includes mathematical tools and algorithms) and Matplotlib. This library provides a selection of efficient tools for machine learning and statistical modeling including classification, regression, clustering and dimensionality reduction (119).

During the pre-processing phase, OpenCV and MoviePy, a video editing tool that can handle basic operations, were used to resize the videos and reduce the computational burden. The code simply cuts the height value in half. The width is then computed so that the width/height ratio is conserved. After resizing, video stabilization was essential to have smoother videos and more consistent tracking. OpenCV and NumPy libraries were used. Two video frames were captured, and the motion between the frames was estimated and corrected.

The next steps involved selecting the ROIs and obtaining the fluorescence intensity information over time after a tracking session. NumPy, OpenCV, and Matplotlib libraries were used. The dimensions of the ROIs (N, vertical and M, horizontal) were set to 5x5 pixels, while the number (n) of ROIs to 300. The ROIs were tracked using the OpenCV library. Specifically, the CRST (Discriminative Correlation Filter with Channel and Spatial Reliability) tracker was chosen due to its balanced performance in terms of both accuracy and speed. The ROIs section of the frame was switched from RGB to HSV color space and the mean of green intensity in the ROIs was obtained. To select randomly the ROIs and start the tracking algorithm, the "s" key on the keyboard is pressed, while pressing the “q” key can prematurely stop execution. The ICG intensity-time curves and the Q and P matrices, which contain information about the light intensity values over time and the coordinates of the selected ROIs in the video, were stored at the end of the execution, which takes a few hours. The outcomes were saved as figures and matrices in a CSV file. Afterwards, the matrices were combined into a single 8100x898 matrix. This included all 27 videos, with each video represented by rows corresponding to the ROIs and columns corresponding to frames.

The fluorescence-time curves underwent pre-processing, including filtering and normalization. A Savitzky–Golay filter is a digital filter that can be applied to a set of digital data points for the purpose of smoothing the data, that is, to increase the precision of the data without distorting the signal tendency (120). Using Scikit-Learn, the dataset was normalized by subctracting the mean (μ) from the input data (x) and dividing it by the standard deviation (σ) along the columns.

Finally, K-means and SOM algorithms were utilized for clustering. A Pytorch implementation of the K-means clustering technique was employed. PyTorch is a machine learning framework built on the Torch library and used for applications like computer vision and natural language processing (96). The MiniSom library was employed to perform SOM clustering. Based on the only study published in the literature (105), the number of clusters was set to 25. The performance of the algorithms was evaluated using the Silhouette score.

Chapter 4

Results

This chapter shows the results achieved using both K-means and SOM algorithms for clustering of fluorescence intensity-time curves.

Twenty-seven surgical videos each were analyzed, excluding those that had significant interference during angiography recording. Actually, when hands or surgical instruments pass in front of the camera or if there are sudden camera movements, the tracking of the ROIs within the frames can be interrupted. This interruption results in distorted measurements. Thus, the training dataset for the ML algorithms consisted of 8100 curves made up of 898 elements extracted from 300 ROIs for each of the 27 videos.

Figure 4.1 shows how the curve pattern differs depending on the location of the ROI within the image.

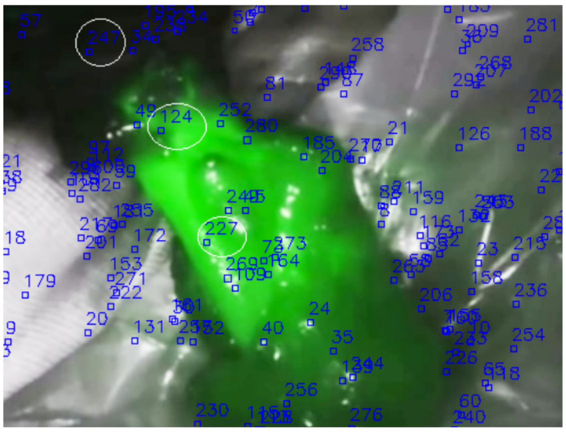

Panel a

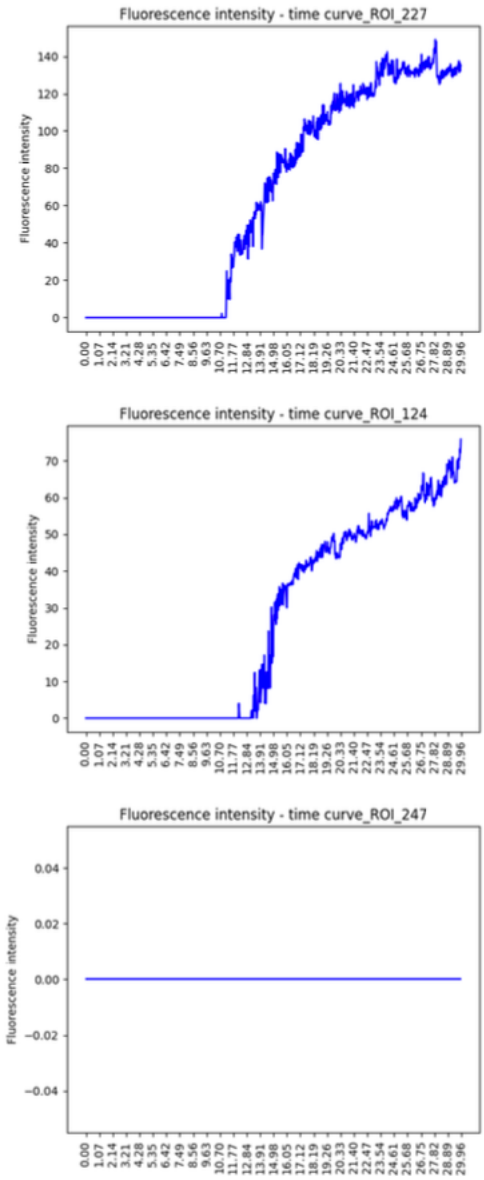

Panel b

Fig. 4.1 ICG fluorescence angiography (panel a) and graphs of the ICG curves of some ROIs at different positions on the bowel (panel b). In each graph, the x-axis represents time (s), and the y-axis shows fluorescence intensity (AU).

4.1 K-means

K-means clustering algorithm requires each cluster to be created based on centroids, which are representative points of the reference class. Figure 4.2 shows the 25 clusters obtained with the K-means algorithm, while the reference centroids for each cluster of ICG curves are depicted in Fig. 4.3.

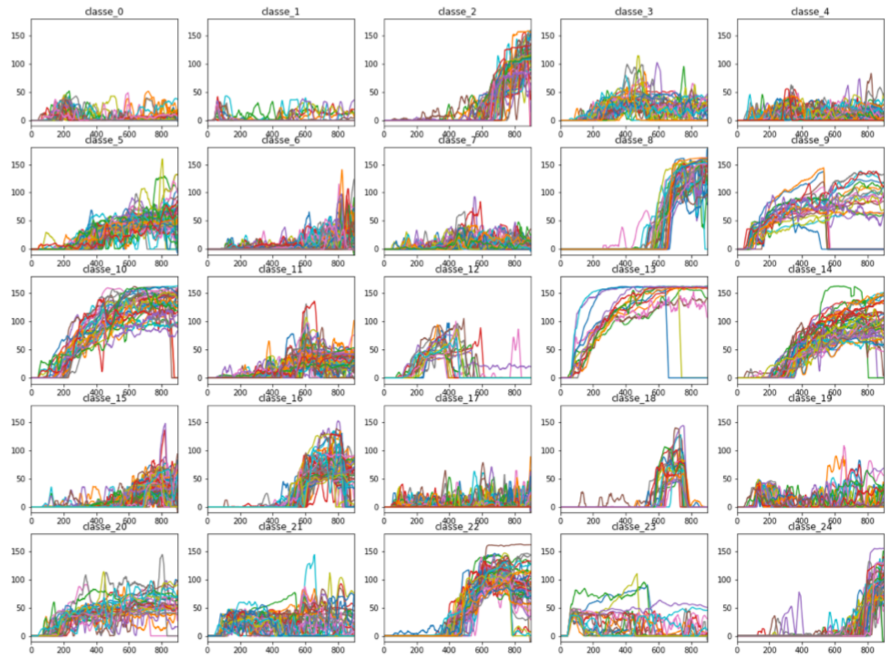

Fig. 4.2 Indocyanine green curve patterns, categorized as a consequence of K-means clustering

Good perfusion is identified by a fluorescence-time curve as that shown in Figure 2.3. A few clusters, such as 10 and 14, exhibit a similar trend to that of the expectations.

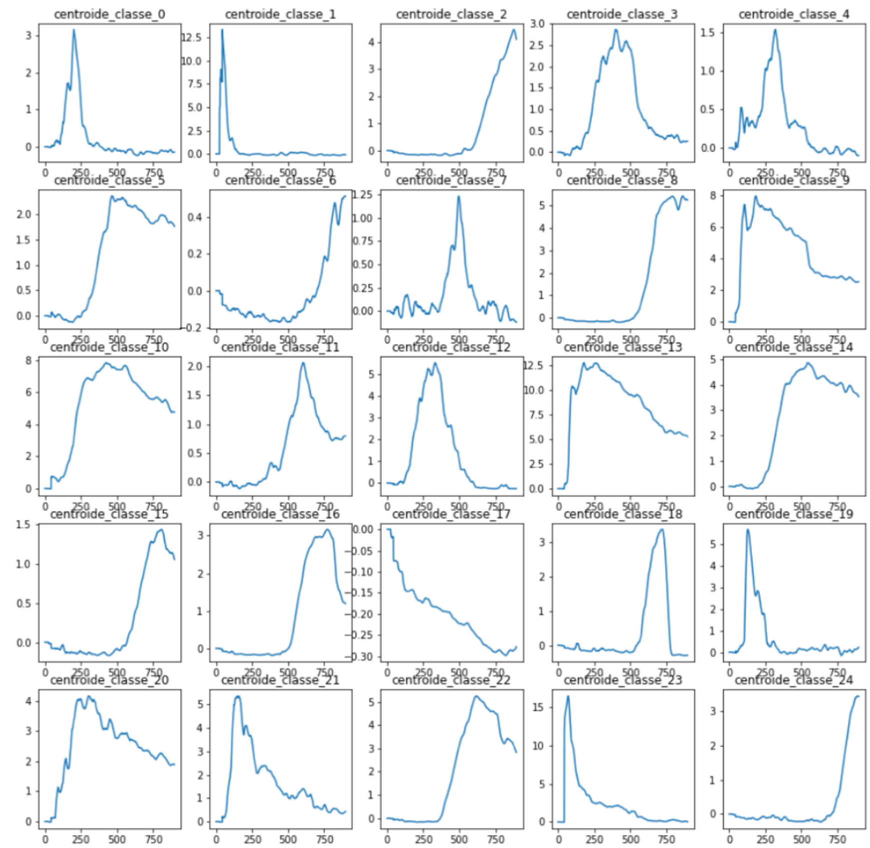

Fig. 4.3 Classified indocyanine green curve centroids as the results of K- means clustering.

4.2 SOM

SOM involves the creation of clusters on the basis of the vectors of the weights, which are supposed to represent the trend of the cluster. Figure 4.4 shows the 25 clusters obtained with the SOM algorithm. The vectors of the weights for the various classes realized by SOM clustering are shown in Figure 4.5

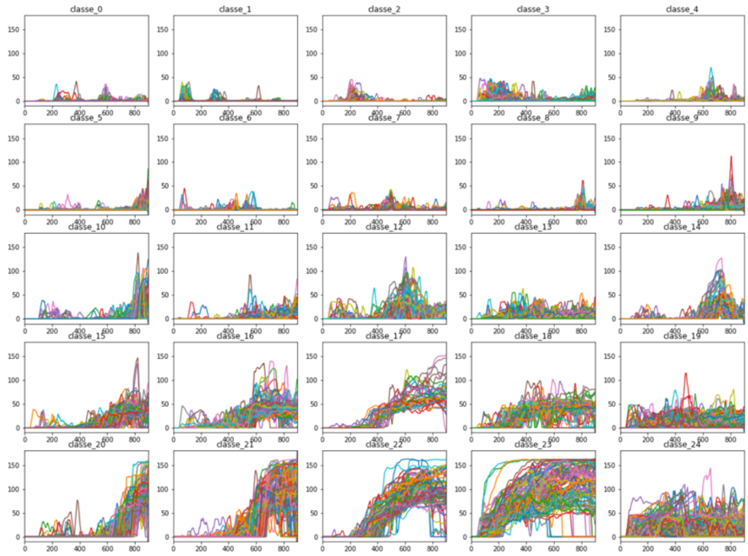

Fig. 4.4 Indocyanine green curve patterns as a consequence of SOM clustering

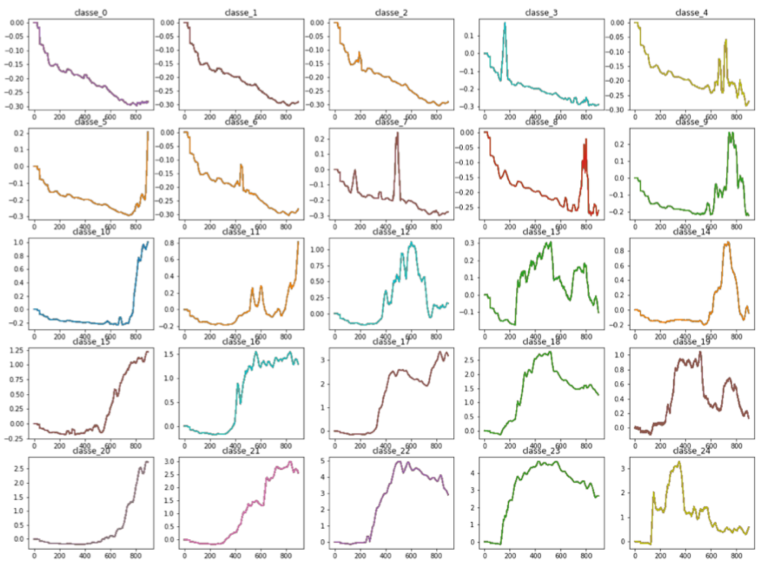

Fig. 4.5 Indocyanine green curve weight vectors

A matrix displaying the occurrences of different classes and the locations of the weight vector centers can be seen in Figure 4.6.

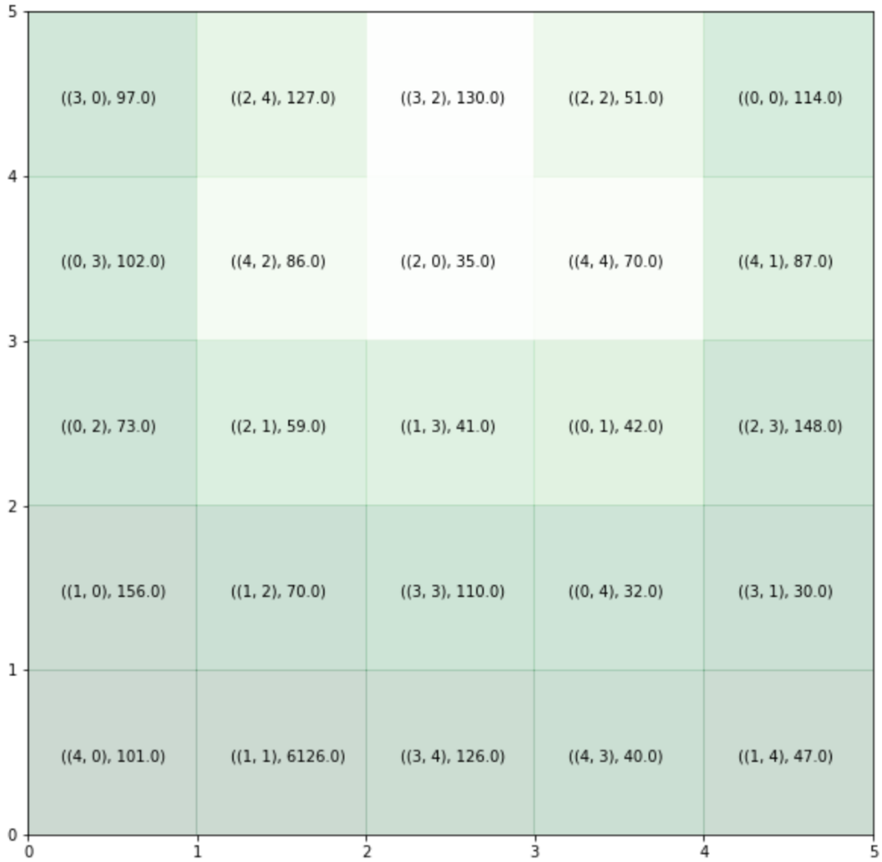

Fig. 4.6 Occurrence matrix. Depending on the similarity between a class and its neighboring cells, the intensity of the cell color increases.

4.3 Comments

When examining the clustering results, the following observations may be made:

- curves near the transection zone have a longer latency period because it takes more time for the fluorescence dye to reach that area compared to more proximal areas in the colonic stump;
- some curves have peaks as a result of environmental issues caused by reflections from the operating room lighting;
- several ROIs shown a fluoresce–time curve that appears significantly different from the reference curve and is less intense because some sections of the operational plane reflect green light;
- some curves ended prematurely due to a sudden movement of the camera, causing the tracker to lose its ROI;
- one class is noticeably more populated than the others, with 6126 curves in the occurrence matrix for the SOM. All curves that are a part of the backdrop ROIs are contained in this class;
- some clusters show a curved pattern which closely resembles the one observed in well-perfused areas, as reported in the only study found in the literature (105).

4.4 Cluster validation

The performance of the clustering methods was evaluated using the silhouette score. Table 4.1 shows the results of the 25 tests conducted for each algorithm. The coefficients for both types of clustering are strong and positive, indicating that the clusters are clearly distinct from each other. The mean silhouette coefficient for K-means was 0.760 ± 0.007, while the SOM showed more variation, with a mean of 0.628 ± 0.052.

Trials	K-means	SOM
run 1	0.770	0.693
run 2	0.758	0.627
run 3	0.762	0.638
run 4	0.761	0.617
run 5	0.760	0.636
run 6	0.767	0.583
run 7	0.756	0.635
run 8	0.778	0.632
run 9	0.754	0.637
run 10	0.751	0.657
run 11	0.760	0.672
run 12	0.754	0.678
run 13	0.755	0.652
run 14	0.758	0.616
run 15	0.761	0.672
run 16	0.755	0.639
run 17	0.751	0.676
run 18	0.750	0.643
run 19	0.769	0.621
run 20	0.767	0.639
run 21	0.761	0.475
run 22	0.762	0.618
run 23	0.762	0.657
run 24	0.762	0.482
run 25	0.755	0.601

Note: The number of runs is entirely random.

Table 4.1. Silhouette Coefficient for K-means and SOM

Conclusions

This thesis work involved a close cooperation between clinicians and surgeons. It represents the current state of a research project aiming to develop a ML-based decision-support system that can automatically and objectively evaluate the quality of bowel perfusion during colorectal surgery. The introduction of such a system into surgical practice is an ambitious goal. However, it can provide valuable indications during surgery, particularly for less experienced surgeons, ultimately enhancing postoperative outcomes and benefiting both patients and the healthcare system.

The research project started by using AI to assess bowel perfusion through fluorescence intensity. Then the focus shifted towards a more complex issue, namely the trend of fluorescence intensity over time. For this purpose, videos of colorectal surgeries were retrieved and, after preprocessing, used to extract fluorescence intensity-time curves from multiple ROIs. K-means and SOM clustering were performed to obtain curve patterns. The subsequent step will be to perform risk labelling on each classified pattern using data on patient complication. Therefore, the learned network will be able to assess the risk and determine whether a region of the bowel, particularly the anastomosis, is properly or improperly perfused. This system may also be developed to provide the optimal bowel transection line as the output.

When evaluating the performance of both algorithms, neither one outperformed the other by a large margin. After 25 trials, the Silhouette coefficients were quite stable and reached a mean of 0.760 and 0.628. Clustering may be further improved. Indeed, there are several challenges involved in video acquisition, image presentation, and algorithm development. Environmental factors have affected the accuracy of measurements. As a matter of facts, it may be challenging to apply an optimally standardized acquisition method in the operating room. This negatively impact the size and quality of the dataset. The passing of hands or surgical instruments can interrupt the tracking of the ROIs within the frames and should be minimized. Using a mechanical holding arm can help maintain a consistent distance and minimize sudden camera movements. Environmental light, even in small amounts, can cause inconsistencies in data acquisition. Although using HSV made the algorithm less sensitive to image lightness, this issue could be more specifically addressed through normalization during the data acquisition process. To ensure a consistent blood flow in the bowel wall, which affects the fluorescence intensity, it may be possible to continuously monitor systemic perfusion factors using an advanced platform. This will help maintain their stability within a predetermined range. Another issue is the placement of the ROIs, as many of them are not positioned within the bowel area, which results in obtaining information only from the background. A potential future development could involve evaluating the positioning of the ROIs specifically in the bowel areas. Moreover, the research group is considering acquiring longer videos and performing clustering by using some features of the fluorescence intensity–time curves, such as AUC, time-to-peak, maximum intensity fluorescence, and slope.

Importantly, the clustering process used in this study did not rely on preexisting external software for data acquisition and constitute a good starting point to build a neural network capable of assessing risk for AL. To ensure effective data labeling for classification purposes, it is important to establish a seamless and improved coordination between engineering and operating room activities, preferably in a multicenter setting.

Acknowledgments

I would like to thank all the people who helped me during this doctoral course. In particular, I am deeply grateful to Prof. Egidio De Benedetto, Eng. Sabatina Criscuolo, Prof. Guido De Sena, and Prof. Umberto Bracale.

References

1. Fry RD, Mahmoud NN, Maron DJ, Bleier JI. Colon and rectum. In: Sabiston Textbook of Surgery. 19th ed. Philadelphia, PA: Saunders; 2012. p. 1294–380.
2. Urciuoli I, Pernazza G. Indocyanine Green-Enhanced Fluorescence-Guided Surgery: Lymphatic Navigation, Perfusion Evaluation and Future Perspectives. In: Ceccarelli G, Coratti A, editors. Robotic Surgery of Colon and Rectum. Springer Nature; 2023. p. 189–98.
3. Azzouz LL, Sharma S. Large Intestine. In: StatPearls [Internet]. Treasure Island (FL): StatPearls Publishing; 2023.
4. Skandalakis JE, Kingsnorth AN, Colborn GL, Weidman TA, Skandalakis PN, Skandalakis LJ. Large Intestine and Anorectum. In: Skandalakis JE, Colburn GL, Weidman TA, Foster Jr RS, Kingsworth AN, Skandalakis LJ, et al., editors. Skandalakis' Surgical Anatomy: the Embryologic and Anatomic Basis of Modern Surgery. Athens: Paschalidis Medical Publications, Ltd.; 2004. p. 861–1002.
5. Coffey JC, O'Leary DP. The mesentery: structure, function, and role in disease. Vol. 1, The Lancet Gastroenterology and Hepatology. Elsevier Ltd; 2016. p. 238–47.
6. Carmichael JC, Mills S. Anatomy and Embryology of the Colon, Rectum, and Anus. In: Steele SR, Hull TL, Hyman N, Maykel JA, Read TE, Whitlow CB, editors. The ASCRS Textbook of Colon and Rectal Surgery. Fourth. Springer Cham; 2022. p. 3–28.
7. Lieske B, Ahmad H. Colon Resection. In: StatPearls [Internet]. Treasure Island (FL): StatPearls Publishing; 2023.
8. Bednarski BK. Surgical resection of primary colon cancer. In: Post TW, editor. UpToDate. Waltham, MA: Wolters Kluwer; 2023.

9. Bleday R, Shibata D. Surgical treatment of rectal cancer. In: Post TW, editor. UpToDate. Waltham, MA: Wolters Kluwer; 2023.
10. Monson JRT, Fleming F. Abdominal perineal resection (APR): Open technique. In: Post TW, editor. UpToDate. Waltham, MA: Wolters Kluwer; 2023.
11. Gupta A, Jain Sudhir. Anastomosis in Surgery. In: Jain SK, Stoker DL, editors. Basic Surgical Skills and Techniques. 1st ed. Jaypee Brothers Medical Publishers (P) Ltd.; 2008. p. 52–63.
12. Pine J, Stevenson L, On J. Intestinal stomas. Surgery (Oxford) [Internet]. 2020;38(1):51–7. Available from: https://www.sciencedirect.com/science/article/pii/S0263931919302261
13. Rakinic J, Tsoraides S. Antibiotics, Approaches, Strategy, and Anastomoses. In: Yeo CJ, editor. Shackelford's Surgery of the Alimentary Tract. Seventh Edition. Philadelphia: W.B. Saunders; 2013. p. 2216–30.
14. Harrell AG, Heniford BT. Minimally invasive abdominal surgery: Lux et veritas past, present, and future. Am J Surg. 2005;190(2):239–43.
15. Matsiota Eugenia (Jenny) and Davidson PL. Milestones in Laparoscopic Colon Surgery. In: Kouraklis Gregory and Matsiota E (Jenny), editor. Laparoscopic Colon Surgery: Milestones, Education, & Best Practice [Internet]. Cham: Springer International Publishing; 2021. p. 1–13. Available from: https://doi.org/10.1007/978-3-030-56728-6_1
16. Jacobs M, Verdeja JC, Goldstein HS. Minimally invasive colon resection (laparoscopic colectomy). Surg Laparosc Endosc. 1991;1(33):144–50.
17. Sciuto A, Tammaro N, Pirozzi F. Evolution and Emerging Trends of Laparoscopic Colorectal Cancer Surgery. Vol. 2, Curr Res Surg. 2019.
18. Creavin B, Kelly ME, Ryan ÉJ, Ryan OK, Winter DC. Oncological outcomes of laparoscopic versus open rectal cancer resections: meta-analysis of randomized clinical trials. British Journal of Surgery. 2021;108(5):469–76.
19. Bissolati M, Orsenigo E, Staudacher C. Minimally invasive approach to colorectal cancer: an evidence-based analysis. Vol.

68, Updates in Surgery. Springer-Verlag Italia s.r.l.; 2016. p. 37–46.
20. Singla V, Bhattacharjee H, Gupta E, Singh D, Mishra A, Kumar D. Performance of three-dimensional and ultra-high-definition (4K) technology in laparoscopic surgery: A systematic review and meta-analysis. J Minim Access Surg. 2022;18(2):167.
21. Fried GM. Emerging Technology in Surgery: Informatics, Robotics, and Electronics. In: Townsend CMJr, Beauchamp RD, Evers BM, Mattox KL, editors. Sabiston Textbook of Surgery. 19th ed. Philadelphia, PA: Saunders; 2012. p. 418–28.
22. Weber PA, Merola S, Wasielewski A, Ballantyne GH. Telerobotic-Assisted Laparoscopic Right and Sigmoid Colectomies for Benign Disease. Dis Colon Rectum. 2002 Dec;45(12):1689–96.
23. Hashizume M, Shimada M, Tomikawa M, Ikeda Y, Takahashi I, Abe R, et al. Early experiences of endoscopic procedures in general surgery assisted by a computer-enhanced surgical system. Surgical Endoscopy And Other Interventional Techniques. 2002 Aug 3;16(8):1187–91.
24. De Rosa M, Bugiantella W, Anteritano F, Mariani L, Ermili F, Ceccarelli G. The Evolution of Minimally Invasive Robotic Surgery in the Last 20 Years. Robotic Surgery of Colon and Rectum. Springer Nature; 2023. p. 3–10.
25. Marchegiani F, Siragusa L, Zadoroznyj A, Laterza V, Mangana O, Schena CA, et al. New Robotic Platforms in General Surgery: What's the Current Clinical Scenario? Medicina (B Aires). 2023 Jul 7;59(7):1264.
26. Spinoglio G, Marano A, Priora F, Melandro F, Formisano G. History of Robotic Surgery. In: Spinoglio G, editor. Robotic Surgery Current Applications and New Trends. Milano: Springer; 2015. p. 1–12.
27. Catarci M, Ruffo G, Borghi F, Patriti A, Delrio P, Scatizzi M, et al. Anastomotic leakage after elective colorectal surgery: a prospective multicentre observational study on use of the Dutch leakage score, serum procalcitonin and serum C-reactive protein for diagnosis. BJS Open. 2020 May 29;4(3):499–507.

28. Borghi F, Migliore M, Cianflocca D, Ruffo G, Patriti A, Delrio P, et al. Management and 1-year outcomes of anastomotic leakage after elective colorectal surgery. Int J Colorectal Dis. 2021 May 29;36(5):929–39.
29. Rahbari NN, Weitz J, Hohenberger W, Heald RJ, Moran B, Ulrich A, et al. Definition and grading of anastomotic leakage following anterior resection of the rectum: A proposal by the International Study Group of Rectal Cancer. Surgery. 2010 Mar;147(3):339–51.
30. Teach Me Surgery. Available online https://teachmesurgery.com/perioperative/gastrointestinal/anastomotic-leak/ [Internet]. 2023. Anastomotic Leak.
31. Chiarello MM, Fransvea P, Cariati M, Adams NJ, Bianchi V, Brisinda G. Anastomotic leakage in colorectal cancer surgery. Vol. 40, Surgical Oncology. Elsevier Ltd; 2022.
32. Catarci M, Ruffo G, Borghi F, Patriti A, Delrio P, Scatizzi M, et al. Colorectal surgery in Italy: a snapshot from the iCral study group. Updates Surg. 2019 Jun 1;71(2):339–47.
33. Ha GW, Kim JH, Lee MR. Oncologic Impact of Anastomotic Leakage Following Colorectal Cancer Surgery: A Systematic Review and Meta-Analysis. Ann Surg Oncol. 2017 Oct 12;24(11):3289–99.
34. La Regina D, Di Giuseppe M, Lucchelli M, Saporito A, Boni L, Efthymiou C, et al. Financial Impact of Anastomotic Leakage in Colorectal Surgery. Journal of Gastrointestinal Surgery. 2019 Mar 13;23(3):580–6.
35. Sciuto A, Merola G, Palma GD De, Sodo M, Pirozzi F, Bracale UM, et al. Predictive factors for anastomotic leakage after laparoscopic colorectal surgery. World J Gastroenterol. 2018 Jun 7;24(21):2247–60.
36. Hunter J, Tang W hao, Schein M, Cheetham M, Hicks CW, Efron JE. Leaking gastrointestinal anastomoses. In: Schein M, Rogers PN, Leppäniemi A, Rosin D, editors. Schein's Common Sense Prevention and Management of Surgical Complications. First. tfm Publishing Limited; 2013. p. 91–143.
37. Vignali A, Gianotti L, Braga M, Radaelli G, Malvezzi L, Carlo V Di. Altered microperfusion at the rectal stump is predictive for rectal anastomotic leak. Dis Colon Rectum. 2000 Jan;43(1):76–82.

38. Urbanavičius L. How to assess intestinal viability during surgery: A review of techniques. World J Gastrointest Surg. 2011;3(5):59.
39. De Nardi P, Elmore U, Maggi G, Maggiore R, Boni L, Cassinotti E, et al. Intraoperative angiography with indocyanine green to assess anastomosis perfusion in patients undergoing laparoscopic colorectal resection: results of a multicenter randomized controlled trial. Surg Endosc. 2020 Jan 21;34(1):53–60.
40. Reinhart MB, Huntington CR, Blair LJ, Heniford BT, Augenstein VA. Indocyanine Green: Historical Context, Current Applications, and Future Considerations. Surg Innov. 2016 Apr 10;23(2):166–75.
41. Landsman ML, Kwant G, Mook GA, Zijlstra WG. Light-absorbing properties, stability, and spectral stabilization of indocyanine green. J Appl Physiol. 1976 Apr 1;40(4):575–83.
42. Iwamoto M, Ueda K, Kawamura J. A Narrative Review of the Usefulness of Indocyanine Green Fluorescence Angiography for Perfusion Assessment in Colorectal Surgery. Vol. 14, Cancers. MDPI; 2022.
43. Dupreé A, Rieß H, Detter C, Debus ES, Wipper SH. Utilization of indocynanine green fluorescent imaging (ICG-FI) for the assessment of microperfusion in vascular medicine. Vol. 3, Innovative Surgical Sciences. De Gruyter; 2020. p. 193–201.
44. Zocola E, Meyer J, Liot E, Toso C, Buchs NC, Ris F, et al. Role of near-infrared fluorescence in colorectal surgery. Vol. 27, World Journal of Gastroenterology. Baishideng Publishing Group Inc; 2021. p. 5189–200.
45. Son GM, Ahn HM, Lee IY, Ha GW. Multifunctional indocyanine green applications for fluorescence-guided laparoscopic colorectal surgery. Vol. 37, Annals of Coloproctology. Korean Society of Coloproctology; 2021. p. 133–40.
46. Baiocchi GL, Gheza F, Molfino S, Arru L, Vaira M, Giacopuzzi S. Indocyanine green fluorescence-guided intraoperative detection of peritoneal carcinomatosis:

systematic review. Vol. 20, BMC Surgery. BioMed Central; 2020.

47. Mandovra P, Kalikar V, Patankar R V. Real-Time Visualization of Ureters Using Indocyanine Green During Laparoscopic Surgeries: Can We Make Surgery Safer? Surg Innov. 2019 Aug 1;26(4):464–8.
48. Morrell ALG, Morrell AC, Morrell-Junior AC, Mendes JM, Tustumi F, Morrell AG. Indocyanine green fluorescence imaging in robotic surgery: State of art, tips and tricks in current applications. Arq Gastroenterol. 2021;58(1):61–70.
49. Baiocchi GL, Guercioni G, Vettoretto N, Scabini S, Millo P, Muratore A, et al. ICG fluorescence imaging in colorectal surgery: a snapshot from the ICRAL study group. BMC Surg. 2021 Dec 1;21(1).
50. Emile SH, Khan SM, Wexner SD. Impact of change in the surgical plan based on indocyanine green fluorescence angiography on the rates of colorectal anastomotic leak: a systematic review and meta-analysis. Vol. 36, Surgical Endoscopy. Springer; 2022. p. 2245–57.
51. Meyer J, Joshi H, Buchs NC, Ris F, Davies J. Fluorescence angiography likely protects against anastomotic leak in colorectal surgery: a systematic review and meta-analysis of randomised controlled trials. Surg Endosc. 2022 Oct 1;36(10):7775–80.
52. Liu RQ, Elnahas A, Tang E, Alkhamesi NA, Hawel J, Alnumay A, et al. Cost analysis of indocyanine green fluorescence angiography for prevention of anastomotic leakage in colorectal surgery. Surg Endosc. 2022 Dec 1;36(12):9281–7.
53. Hardy NP, Dalli J, Khan MF, Andrejevic P, Neary PM, Cahill RA. Inter-user variation in the interpretation of near infrared perfusion imaging using indocyanine green in colorectal surgery. Surg Endosc. 2021 Dec 1;35(12):7074–81.
54. Al-Jaroodi J, Mohamed N, Abukhousa E. Health 4.0: On the Way to Realizing the Healthcare of the Future. IEEE Access. 2020;8:211189–210.
55. Carolina A, Monteiro1 B, Padilha R. Health 4.0: Applications, Management, Technologies and Review Type of article: Review. Medical Technologies Journal [Internet]. (2):262–76.

Available from: https://doi.org/10.26415/2572-004X-vol2iss1p262-276
56. Kolcu MİB, Kolcu G. Health 4.0. In: İyigün İ, Görçün ÖF, editors. Health 40 and Medical Supply Chain. Singapore: Springer; 2023. p. 109–19.
57. Sisodia A, Jindal R. A meta-analysis of industry 4.0 design principles applied in the health sector. Vol. 104, Engineering Applications of Artificial Intelligence. Elsevier Ltd; 2021.
58. Lam K, Abràmoff MD, Balibrea JM, Bishop SM, Brady RR, Callcut RA, et al. A Delphi consensus statement for digital surgery. NPJ Digit Med. 2022 Dec 1;5(1).
59. Hardy NP, Cahill RA. Digital surgery for gastroenterological diseases. World J Gastroenterol. 2021 Nov 14;27(42):7240–6.
60. Musacchio N, Guaita G, Ozzello A, Pellegrini MA, Ponzani P, Zilich R, et al. Intelligenza Artificiale e Big Data in ambito medico: prospettive, opportunità. criticità JAMD [Internet]. 2018;21(3). Available from: www.jamd.it
61. Spinelli A, Carrano FM, Laino ME, Andreozzi M, Koleth G, Hassan C, et al. Artificial intelligence in colorectal surgery: an AI-powered systematic review. Vol. 27, Techniques in Coloproctology. Springer Science and Business Media Deutschland GmbH; 2023. p. 615–29.
62. World Health Organisation. Ethics and governance of artificial intelligence for health. 2021.
63. Copeland BJ. Artificial intelligence. In: Encyclopedia Britannica. 2023.
64. Russell S, Norvig P, editors. What Is AI? In: Artificial Intelligence A modern Approach. third. Upper Saddle River, New Jersey: Pearson; 2009. p. 1–33.
65. Hamet P, Tremblay J. Artificial intelligence in medicine. Metabolism. 2017 Apr;69:S36–40.
66. Awad M, Khanna R. Machine Learning. In: Efficient Learning Machines. Berkeley, CA: Apress; 2015. p. 1–18.
67. Hinton GE, Osindero S, Teh YW. A Fast Learning Algorithm for Deep Belief Nets. Neural Comput. 2006 Jul;18(7):1527–54.

68. Sarker IH. Deep Learning: A Comprehensive Overview on Techniques, Taxonomy, Applications and Research Directions. SN Comput Sci. 2021 Nov 18;2(6):420.
69. Mitsala A, Tsalikidis C, Pitiakoudis M, Simopoulos C, Tsaroucha AK. Artificial Intelligence in Colorectal Cancer Screening, Diagnosis and Treatment. A New Era. Current Oncology. 2021 Apr 23;28(3):1581–607.
70. Moglia A, Georgiou K, Georgiou E, Satava RM, Cuschieri A. A systematic review on artificial intelligence in robot-assisted surgery. International Journal of Surgery. 2021 Nov;95:106151.
71. Moglia A, Georgiou K, Morelli L, Toutouzas K, Satava RM, Cuschieri A. Breaking down the silos of artificial intelligence in surgery: glossary of terms. Surg Endosc. 2022 Nov 21;36(11):7986–97.
72. Maier-Hein L, Eisenmann M, Sarikaya D, März K, Collins T, Malpani A, et al. Surgical data science – from concepts toward clinical translation. Med Image Anal. 2022 Feb;76:102306.
73. Quero G, Mascagni P, Kolbinger FR, Fiorillo C, De Sio D, Longo F, et al. Artificial Intelligence in Colorectal Cancer Surgery: Present and Future Perspectives. Cancers (Basel). 2022 Aug 4;14(15):3803.
74. Anteby R, Horesh N, Soffer S, Zager Y, Barash Y, Amiel I, et al. Deep learning visual analysis in laparoscopic surgery: a systematic review and diagnostic test accuracy meta-analysis. Surg Endosc. 2021 Apr 4;35(4):1521–33.
75. Pourahmad S, Pourhashemi S, Mohammadianpanah M. Colorectal Cancer Staging Using Three Clustering Methods Based on Preoperative Clinical Findings. Asian Pacific Journal of Cancer Prevention. 2016 Mar 7;17(2):823–7.
76. Maheshwari K, Cywinski J, Mathur P, Cummings KC, Avitsian R, Crone T, et al. Identify and monitor clinical variation using machine intelligence: a pilot in colorectal surgery. J Clin Monit Comput. 2019 Aug 24;33(4):725–31.
77. Curtis NJ, Dennison G, Salib E, Hashimoto DA, Francis NK. Artificial Neural Network Individualised Prediction of Time to Colorectal Cancer Surgery. Gastroenterol Res Pract. 2019 Jul 9;2019:1–10.
78. Aikemu B, Xue P, Hong H, Jia H, Wang C, Li S, et al. Artificial Intelligence in Decision-Making for Colorectal

Cancer Treatment Strategy: An Observational Study of Implementing Watson for Oncology in a 250-Case Cohort. Front Oncol. 2021 Feb 4;10.
79. Azimi K, Honaker MD, Chalil Madathil S, Khasawneh MT. Post-Operative Infection Prediction and Risk Factor Analysis in Colorectal Surgery Using Data Mining Techniques: A Pilot Study. Surg Infect (Larchmt). 2020 Nov 1;21(9):784–92.
80. Sammour T, Lewis M, Thomas ML, Lawrence MJ, Hunter A, Moore JW. A simple web-based risk calculator (www.anastomoticleak.com) is superior to the surgeon's estimate of anastomotic leak after colon cancer resection. Tech Coloproctol. 2017 Jan 19;21(1):35–41.
81. Sammour T, Cohen L, Karunatillake AI, Lewis M, Lawrence MJ, Hunter A, et al. Validation of an online risk calculator for the prediction of anastomotic leak after colon cancer surgery and preliminary exploration of artificial intelligence-based analytics. Tech Coloproctol. 2017 Nov 1;21(11):869–77.
82. Francis NK, Luther A, Salib E, Allanby L, Messenger D, Allison AS, et al. The use of artificial neural networks to predict delayed discharge and readmission in enhanced recovery following laparoscopic colorectal cancer surgery. Tech Coloproctol. 2015 Jul 3;19(7):419–28.
83. Antunes JT, Ofshteyn A, Bera K, Wang EY, Brady JT, Willis JE, et al. Radiomic Features of Primary Rectal Cancers on Baseline T2-Weighted MRI Are Associated With Pathologic Complete Response to Neoadjuvant Chemoradiation: A Multisite Study. Journal of Magnetic Resonance Imaging. 2020 Nov 26;52(5):1531–41.
84. Nakanishi R, Akiyoshi T, Toda S, Murakami Y, Taguchi S, Oba K, et al. Radiomics Approach Outperforms Diameter Criteria for Predicting Pathological Lateral Lymph Node Metastasis After Neoadjuvant (Chemo)Radiotherapy in Advanced Low Rectal Cancer. Ann Surg Oncol. 2020 Oct 7;27(11):4273–83.
85. Liu M, Ma X, Shen F, Xia Y, Jia Y, Lu J. MRI-based radiomics nomogram to predict synchronous liver metastasis in primary rectal cancer patients. Cancer Med. 2020 Jul 31;9(14):5155–63.

86. Meng X, Xia W, Xie P, Zhang R, Li W, Wang M, et al. Preoperative radiomic signature based on multiparametric magnetic resonance imaging for noninvasive evaluation of biological characteristics in rectal cancer. Eur Radiol. 2019 Jun 9;29(6):3200–9.
87. Kitaguchi D, Takeshita N, Matsuzaki H, Oda T, Watanabe M, Mori K, et al. Automated laparoscopic colorectal surgery workflow recognition using artificial intelligence: Experimental research. International Journal of Surgery. 2020 Jul;79:88–94.
88. Baltussen EJM, Brouwer de Koning SG, Sanders J, Aalbers AGJ, Kok NFM, Beets GL, et al. Tissue diagnosis during colorectal cancer surgery using optical sensing: an in vivo study. J Transl Med. 2019 Dec 2;17(1):333.
89. Shademan A, Decker RS, Opfermann JD, Leonard S, Krieger A, Kim PCW. Supervised autonomous robotic soft tissue surgery. Sci Transl Med. 2016 May 4;8(337).
90. Adams K, Papagrigoriadis S. Creation of an effective colorectal anastomotic leak early detection tool using an artificial neural network. Int J Colorectal Dis. 2014 Apr 12;29(4):437–43.
91. Weller GB, Lovely J, Larson DW, Earnshaw BA, Huebner M. Leveraging electronic health records for predictive modeling of post-surgical complications. Stat Methods Med Res. 2018 Nov 1;27(11):3271–85.
92. Park JH, Baek JH, Sym SJ, Lee KY, Lee Y. A data-driven approach to a chemotherapy recommendation model based on deep learning for patients with colorectal cancer in Korea. BMC Med Inform Decis Mak. 2020 Dec 22;20(1):241.
93. Blansit K, Marmor R, Zhao B, Tien D. Voice Enabled Framework to Support Post-Surgical Discharge Monitoring. AMIA Annu Symp Proc. 2017;2017:2274–8.
94. Lütken CD, Achiam MP, Svendsen MB, Boni L, Nerup N. Optimizing quantitative fluorescence angiography for visceral perfusion assessment. Surg Endosc. 2020 Dec 21;34(12):5223–33.
95. Lütken CD, Achiam MP, Osterkamp J, Svendsen MB, Nerup N. Quantification of fluorescence angiography: Toward a reliable intraoperative assessment of tissue perfusion - A narrative review. Langenbecks Arch Surg. 2021 Mar 21;406(2):251–9.

96. Brownson JRS. Laws of Light. In: Solar Energy Conversion Systems. 1st ed. Cambridge, MA: Academic Press; 2013. p. 41–66.
97. Nerup N, Knudsen KBK, Ambrus R, Svendsen MBS, Thymann T, Ifaoui IBR, et al. Reproducibility and Reliability of Repeated Quantitative Fluorescence Angiography. Surg Technol Int. 2017 Nov 9;31:35–9.
98. Nerup N, Andersen HS, Ambrus R, Strandby RB, Svendsen MBS, Madsen MH, et al. Quantification of fluorescence angiography in a porcine model. Langenbecks Arch Surg. 2017 Jun 15;402(4):655–62.
99. Quero G, Lapergola A, Barberio M, Seeliger B, Saccomandi P, Guerriero L, et al. Discrimination between arterial and venous bowel ischemia by computer-assisted analysis of the fluorescent signal. Surg Endosc. 2019 Jun 16;33(6):1988–97.
100. Wada T, Kawada K, Takahashi R, Yoshitomi M, Hida K, Hasegawa S, et al. ICG fluorescence imaging for quantitative evaluation of colonic perfusion in laparoscopic colorectal surgery. Surg Endosc. 2017 Oct 9;31(10):4184–93.
101. Son GM, Kwon MS, Kim Y, Kim J, Kim SH, Lee JW. Quantitative analysis of colon perfusion pattern using indocyanine green (ICG) angiography in laparoscopic colorectal surgery. Surg Endosc. 2019 May 10;33(5):1640–9.
102. Gomez-Rosado JC, Valdes-Hernandez J, Cintas-Catena J, Cano-Matias A, Perez-Sanchez A, del Rio-Lafuente FJ, et al. Feasibility of quantitative analysis of colonic perfusion using indocyanine green to prevent anastomotic leak in colorectal surgery. Surg Endosc. 2022 Feb 6;36(2):1688–95.
103. Cahill RA, O'Shea DF, Khan MF, Khokhar HA, Epperlein JP, Mac Aonghusa PG, et al. Artificial intelligence indocyanine green (ICG) perfusion for colorectal cancer intra-operative tissue classification. British Journal of Surgery. 2021 Jan 27;108(1):5–9.
104. Hardy NP, Epperlein JP, Dalli J, Robertson W, Liddy R, Aird JJ, et al. Real-time administration of indocyanine green in combination with computer vision and artificial intelligence for

the identification and delineation of colorectal liver metastases. Surg Open Sci. 2023 Mar;12:48–54.

105. Park SH, Park HM, Baek KR, Ahn HM, Lee IY, Son GM. Artificial intelligence based real-time microcirculation analysis system for laparoscopic colorectal surgery. World J Gastroenterol. 2020 Nov 28;26(44):6945–62.
106. Arpaia P, Bracale U, Corcione F, De Benedetto E, Di Bernardo A, Di Capua V, et al. Assessment of blood perfusion quality in laparoscopic colorectal surgery by means of Machine Learning. Sci Rep. 2022 Aug 29;12(1):14682.
107. Mishra S. https://towardsdatascience.com/unsupervised-learning-and-data-clustering-eeecb78b422a. 2017. Unsupervised Learning and Data Clustering.
108. Gentleman R, Carey VJ. Unsupervised Machine Learning. In: Bioconductor Case Studies. New York, NY: Springer New York; 2008. p. 137–57.
109. James G, Witten D, Hastie T, Tibshirani R, editors. Unsupervised learning. In: An Introduction to Statistical Learning with Applications in R. 2nd ed. New York: Springer; 2021. p. 497–552.
110. Hayasaka S. What is Clustering and How Does it Work? 2021. k-Means Clustering.
111. Ponmalai R, Kamath C, editors. What Is a Self-Organizing Map and When Should It Be Used? In: Self-Organizing Maps and Their Applications to Data Analysis. Livermore, CA: Lawerence Livermore National Laboratory; 2019.
112. Wehrens R. 2.28 - Data Mapping: Linear Methods versus Nonlinear Techniques. In: Brown SD, Tauler R, Walczak B, editors. Comprehensive Chemometrics [Internet]. Oxford: Elsevier; 2009. p. 619–33. Available from: https://www.sciencedirect.com/science/article/pii/B978044452701100065X
113. Khazri A. Towards Data Science. 2019. Self Organizing Maps.
114. Aldrich C, Auret L. Artificial Neural Networks. In: Unsupervised Process Monitoring and Fault Diagnosis with Machine Learning Methods. London: Springer London; 2013. p. 71–115.
115. Akman O, Comar T, Hrozencik D, Gonzales J. Chapter 11 - Data Clustering and Self-Organizing Maps in Biology. In:

Robeva R, Macauley M, editors. Algebraic and Combinatorial Computational Biology [Internet]. Academic Press; 2019. p. 351–74. (MSE/Mathematics in Science and Engineering). Available from: https://www.sciencedirect.com/science/article/pii/B9780128140666000118

116. Dudek A. Silhouette Index as Clustering Evaluation Tool. In 2020. p. 19–33.
117. Hou J, Ye X, Li C, Wang Y. K-Module Algorithm: An Additional Step to Improve the Clustering Results of WGCNA Co-Expression Networks. Genes (Basel). 2021 Jan 12;12(1):87.
118. Available online https://aws.amazon.com/what-is/python/?nc1=h_ls [Internet]. What is Python?
119. Available online https://www.tutorialspoint.com/scikit_learn/ [Internet]. Scikit Learn Tutorial.
120. Available online https://en.wikipedia.org/wiki/Savitzky–Golay_filter [Internet]. Savitzky–Golay filter.